J. Phys. France 49 (1988) 1875-1899 NOVEMBRE 1988, PAGE 1875

Classification
Physics Abstracts
61.30G — 05.70L — 47.20 — 47.65

On electrically driven pattern-forming instabilities in planar nematics

Eberhard Bodenschatz, Walter Zimmermann and Lorenz Kramer

Physikalisches Institut der Universität Bayreuth D-8580 Bayreuth, F.R.G.

(*Reçu le 25 avril 1988, accepté le 11 juillet 1988*)

Résumé. — Nous reconsidérons la description théorique du comportement au seuil et près du seuil de la convection électrohydrodynamique des cristaux liquides nématiques dans le régime de conduction (basse fréquence). Nous présentons essentiellement l'analyse linéaire tridimensionnelle complète de l'état de base ainsi qu'une grande partie de la théorie faiblement non linéaire de l'état convectif. Les conditions aux limites aux plaques supérieure et inférieure et la dépendance du temps sont traitées rigoureusement ; l'effet flexoélectrique est toutefois négligé. Nous étendons notre analyse à différentes transitions, comme l'instabilité de splay-twist périodique qui survient dans les matériaux polymères avec une anisotropie diélectrique positive. Nous donnons des critères pour l'observation de l'état des rouleaux obliques et pour la compétition entre différentes instabilités. Dans la mesure du possible, nous comparons nos résultats théoriques avec l'expérience en insistant sur l'accord qualitatif, parfois quantitatif, que nous avons trouvé.

Abstract. — The theoretical description of the threshold and near-threshold behavior of electrohydrodynamic convection in nematic liquid crystals in the (low-frequency) conduction regime is reconsidered. We present essentially the full three-dimensional linear stability analysis of the basic state and a major part of the weakly-nonlinear theory of the convective state. Boundary conditions at the upper and lower plates as well as the time dependence are treated rigorously but the flexoelectric effect is neglected. Related transitions like the periodic splay-twist instability, which is relevant in polymer materials with positive dielectric anisotropy, are also considered. We give criteria for finding the oblique-roll state and for the competition between different instabilities. Comparison with experiments is made wherever possible. Good qualitative and sometimes quantitative agreement is found.

1. Introduction.

When a low-frequency alternating voltage is applied across a thin layer of nematic liquid crystal having negative or slightly positive dielectric anisotropy, sufficient (ionic) conductivity, and uniform orientation of the director $\hat{n}$ in the plane of the layer, an instability of the basic unstructured state occurs which under ideal conditions leads to a periodic pattern of convection rolls (for reviews see [1, 2]). There is a sharp and reversible threshold for this phenomenon which is typically between 5 and 10 Volts. When the voltage is increased further one usually finds either transitions to more complicated spatio-temporal states which are heavily influenced by defects [3, 4], or, if the increase is performed adiabatically slow, well defined secondary transitions to essentially ideal structures, which in most cases are periodic in two directions [5, 6]. At sufficiently high voltage transitions to turbulence occur (often called the dynamic-scattering mode).

This electrohydrodynamic convection (EHC) in nematics has a number of properties which distinguishes it from other convective instabilities like the thermally driven Rayleigh-Bénard convection in simple fluids [7], which has been studied more intensively :

i) Because of the small thickness of the layers in EHC (usually $\sim 5 - 200\ \mu m$) the relaxation times are short and one can easily produce specimens with large aspect ratios (= ratio of lateral dimension to thickness) in one or two directions.

ii) In addition to the amplitude of the applied voltage one has the frequency as an easily accessible external control parameter. This, together with the facts that the material couples strongly to an additional magnetic field and that a vast variety of

nematics with different material constants are available, provides for very rich scenarios. Unfortunately, only for very few nematics all the parameters are known and there is often the problem of deterioration and contamination of the specimens.

iii) As a result of the planar anchoring of the director at the upper and lower plates that hold the layer there is an axial anisotropy, so that the patterns orient with respect to the preferred axis. At the first threshold only rolls or possibly a rectangular structure are expected to appear [8, 9]. The existence and stability of roll solutions above threshold should now be considered in terms of 2-dimensional wavevector regions instead of the wavenumber bands adequate for isotropic systems.

Unfortunately the theoretical description of EHC is very complicated due to the complexity of the underlying hydrodynamic equations. The fact that the external driving is time dependent (ac voltage) adds to the complication. As a result only the linear threshold for a pattern of stationary rolls that is normal to the undistorted director (the so-called « Williams-domains ») can be considered understood in the low-frequency range (« conduction regime »). No systematic treatment of the nonlinear behavior above threshold is available.

Generalizations of the theoretical description are highly desirable, even in the conduction regime. On the one hand the observation of stationary oblique rolls (or « Zigzag » structures) [5, 6] and of travelling rolls at the first threshold [10] necessitate a generalization of the linear threshold calculations. On the other hand a systematic treatment of the nonlinear effects would allow one to understand the possible structures, defects and transitions at least slightly above threshold in the « weakly-nonlinear » region. As an example we point out the undulated roll structure observed in the vicinity of the normal-oblique transition [5, 6]. The weakly-nonlinear analysis is a standard technique that has been applied successfully to many other pattern-forming systems [11], which would then put EHC into the general framework of current ideas on pattern-formation and -selection [12].

In this paper a solution to some of the above problems is presented. In section 2 the basic hydrodynamic equations neglecting the flexoelectric effect [12a] are collected and in section 3 the full three-dimensional linear theory that allows one to describe the first threshold as well as the structure at threshold (up to degeneracies) and the fastest-growing modes above threshold is formulated. The appropriate modal analysis and some approximations pertaining to the spatial dependence of the modes across the layer (essentially connected with boundary conditions) and to the time-dependence, which is mostly treated by Fourier expansion, are introduced.

In section 4 the results of the linear analysis, which have been published in part previously [13], are presented. A lowest-order time-Fourier approximation valid when the director and the velocities fluctuate only weakly with the external frequency is used in connection with free and (realistic) rigid boundary conditions (Subsect. 4.1 and 4.2). The « full » Fourier expansion in subsection 4.3 is used only in connection with free boundary conditions and with trial functions that approximate rigid boundary conditions. Although in the formulation of the analysis in section 3 Hopf bifurcations, leading to moving patterns, and the modes for the dielectric regime are included, we leave a detailed investigation of these effects to future work (see also the discussion in Sect. 6). The oblique rolls can be explained and interesting predictions for scenarios in the presence of magnetic fields applied in the plane of the layer and in very thin and clean specimens (here one needs the full Fourier expansion) are made. For materials with positive dielectric anisotropy the competition of EHC with the homogeneous Fréedericksz transition and with the periodic splay-twist transition discovered recently in polymer materials [14-17] is discussed. Since the periodic splay-twist transition comes out naturally in our framework we discuss it in subsection 4.4 and present new results on the influence of additional fields.

In section 5, finally, the weakly nonlinear analysis is presented. We have calculated the amplitude of the pattern slightly above threshold for normal rolls and compared it to existing experiments. We always found a supercritical bifurcation. The parameters for the universal amplitude (or envelope) equations that apply to this type of anisotropic system [8, 9] in the absence of mean-flow effects [18, 19] are given. These equations describe the threshold pattern and slow variations in time and space around it. Among others they allow the determination of the stable wavevector regions of roll solutions, describe point and line defects and exhibit stable undulated roll solutions.

Some technical details are deferred to the Appendices. In Appendix A the calculations for the trial-function approximation for rigid boundary conditions is presented. In Appendix B a method to treat the low-frequency limit for the ac voltage is exhibited. Appendix C is devoted to the rigorous treatment of the time dependence by Fourier expansion and in Appendix D two sets of material parameters for the standard material MBBA used by us are tabulated.

2. Basic equations.

The electrohydrodynamic equations of nematic liquid crystals consist of the hydrodynamic equations

(mass conservation, balance of momentum and of angular momentum) (see e.g. [1]) and of the quasi-static Maxwell equations (charge conservation, Coulomb's law) together with suitable (linear) constitutive relations. The static properties are conveniently expressed in terms of a free energy density whose orientational elastic part is given by [20-23]

$$F_{el} = \frac{1}{2}\,[k_{11}(\nabla\cdot\hat{n})^2 + k_{22}(\hat{n}\cdot\nabla\times\hat{n})^2 + k_{33}(\hat{n}\times\nabla\times\hat{n})^2] \quad (2.1)$$

The elastic constants k_{11}, k_{22} and k_{33} pertain to splay, twist and bend deformations, respectively.

The magnetic susceptibility and dielectric tensors are uniaxial and can be written in Cartesian coordinates in the form

$$\begin{aligned} \chi_{ij} &= \chi_\perp\,\delta_{ij} + \chi_a\,n_i\,n_j\,,\ \chi_a = \chi_\parallel - \chi_\perp \\ \varepsilon_{ij} &= \varepsilon_\perp\,\delta_{ij} + \varepsilon_a\,n_i\,n_j\,,\ \varepsilon_a = \varepsilon_\parallel - \varepsilon_\perp\,. \end{aligned} \quad (2.2)$$

The magnetic anisotropic part χ_a is usually positive, whereas ε_a can be either positive or negative. Then the director-dependent parts of the magnetic and dielectric free energies are

$$F_{em} = -\frac{1}{2}\,\mu_0\,\chi_a(\hat{n}\cdot\mathbf{H})^2 - \frac{1}{2}\,\varepsilon_0\,\varepsilon_a(\hat{n}\cdot\mathbf{E})^2 \quad (2.3)$$

where μ_0 and ε_0 are the permeability and the dielectric constant of the vacuum.

The balance of torques acting on the director can now be written as [24-26]

$$\begin{aligned} \boldsymbol{\Gamma} &= \hat{n}\times\mathbf{S} = 0\,, \\ \mathbf{S} &= -\,[\delta F/\delta\hat{n} + (\gamma_1\,\mathbf{N} + \gamma_2\,\mathbf{A}\hat{n})]\,, \end{aligned} \quad (2.4)$$

where inertial terms involving the second time-derivative of $\hat{n}$ are neglected as usual. The first term in the expression for $\mathbf{S}$ gives the torque due to elastic, magnetic and dielectric forces with the functional derivative $\delta/\delta n_i = \partial n_i - \partial_j(\partial n_{i,j})$ (the notation $\partial_j = \partial x_j$, $n_{i,j} = \partial_j n_i$ will be used freely). The viscous torque due to fluid motion is given in the other terms of equation (2.4), with $\mathbf{N} = \mathrm{d}\hat{n}/\mathrm{d}t + 1/2\,\hat{n}\times(\nabla\times\mathbf{v})$ the rate of change of the director relative to the moving fluid ($\mathrm{d}/\mathrm{d}t = \partial_t + \mathbf{v}\cdot\nabla$ is the substantial time derivative), $A_{i,j} = 1/2(v_{j,i} + v_{i,j})$ the symmetric strain tensor and γ_1, γ_2 the rotational viscosities.

Actually equation (2.4) involves only two components. To make this explicit in a general situation one may introduce spherical polar coordinates for the director

$$\hat{n}(\mathbf{r}) = (\cos\theta\cos\psi, \cos\theta\sin\psi, \sin\theta) \quad (2.5)$$

and an orthogonal transformation

$$\mathbf{D} = \begin{bmatrix} \cos\theta\cos\psi & \cos\theta\sin\psi & \sin\theta \\ -\sin\psi & \cos\psi & 0 \\ -\sin\theta\cos\psi & -\sin\theta\sin\psi & \cos\theta \end{bmatrix} \quad (2.6)$$

which transforms the x-axis into the $\hat{n}$-axis. A straight-forward evaluation of the transformed torque $\boldsymbol{\Gamma}' = \mathbf{D}\boldsymbol{\Gamma}$ then shows that Γ_1' vanishes trivially and

$$\begin{aligned} \Gamma_2' &= \sin\theta\,(S_x\cos\psi + S_y\sin\psi) - S_z\cos\theta\,, \\ \Gamma_3' &= -\,S_x\sin\psi + S_y\cos\psi\,. \end{aligned} \quad (2.7)$$

From momentum balance follows the equation of motion [23-26]

$$\rho_m\,\mathrm{d}v_i/\mathrm{d}t = f_i + \partial T_{\ell i}/\partial x_\ell \quad (2.8)$$

(ρ_m = mass density). The volume force $\mathbf{f}$ is in our case

$$\mathbf{f} = \rho_e\,\mathbf{E} \quad (2.9)$$

(ρ_e = charge density, $\mathbf{E}$ = electric field) and the stress tensor is

$$\mathbf{T}_{ij} = -\,p\delta_{ij} - (\delta F/\delta n_{k,i})\,n_{k,j} + t_{ij} \quad (2.10)$$

(p = pressure). The second term on the r.h.s. is of second order in the deformations of $\hat{n}$ and thus drops out of the linearized equations considered in the next section. The general form of the viscous stress tensor contains six viscosity coefficients [25, 23, 26]

$$t_{ij} = \alpha_1\,n_k\,n_\ell\,A_{k\ell}\,n_i\,n_j + \alpha_2\,n_i\,N_j + \alpha_3\,n_j\,N_i + \alpha_4\,A_{ij} + \alpha_5\,n_i\,n_k\,A_{kj} + \alpha_6\,n_j\,n_k\,A_{ki}\,. \quad (2.11)$$

The isotropic viscosity corresponds to $\alpha_4/2$. A nice visualization of the other viscosities is presented in reference [27]. From the Onsager reciprocity relations follows [28]

$$\alpha_6 - \alpha_5 = \alpha_2 + \alpha_3\,. \quad (2.12)$$

For constraints on the α_i due to thermodynamic stability see e.g. [29, 26]. The rotational viscosities can be expressed in terms of the (shear) viscosities

$$\gamma_1 = \alpha_3 - \alpha_2\,,\quad \gamma_2 = \alpha_3 + \alpha_2\,. \quad (2.13)$$

The fluid will be treated as incompressible so that

$$\nabla\cdot\mathbf{v} = 0\,. \quad (2.14)$$

Finally we have the equations of electrostatics

$$\nabla\cdot(\boldsymbol{\varepsilon}\mathbf{E}) = \rho_e\,,\quad \nabla\times\mathbf{E} = 0\,, \quad (2.15)$$

and charge conservation

$$\nabla\cdot\mathbf{j} + \partial_t\rho_e = 0\,,\quad \mathbf{j} = \underset{\sim}{\sigma}\mathbf{E}\,\rho_e\mathbf{v}\,, \quad (2.16)$$

where the conductivity tensor $\boldsymbol{\sigma}$ has the same form as $\boldsymbol{\chi}$ and $\boldsymbol{\varepsilon}$ (see Eq. (2.2)). In most cases σ_a is positive.

It is convenient to eliminate the pressure by taking the curl of the momentum equation (2.8) and to eliminate the charge density from equation (2.8) and

from the equation of charge conservation (2.16) with the help of the first equation (2.15) (Coulomb's law). The second equation of (2.15) is satisfied by writing

$$\mathbf{E} = \mathbf{E}_0 - \nabla\phi \tag{2.17}$$

where $\mathbf{E}_0$ is the applied electric field. One is then left with six equations (two from (2.4), two from (2.8), as well as (2.14) and (2.16)) for the quantities ϕ, θ, ψ, v_x, v_y, v_z.

We consider a nematic slab of thickness d (Fig. 1) and now turn to the question of boundary conditions at the upper and lower plates. All lengths (velocities

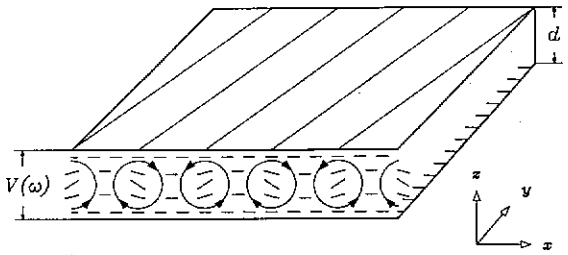

Fig. 1. — Sketch of the geometry and the periodic convection structure.

included) will be measured from now on in units of d/π so that the plates are at $z = \pm \pi/2$. On each plate one boundary condition is needed for each quantity. The conditions

$$\phi = v_z = 0\,, \quad z = \pm \pi/2 \tag{2.18}$$

result from the geometric constraint and will always be assumed to hold. The condition

$$\theta = 0\,, \quad z = \pm \pi/2 \tag{2.19}$$

results from the assumption of strong anchoring with respect to splay deformations at the boundaries. Condition (2.19) will always be used. Analysis is usually simplified by taking (unrealistic) torque-free and stress-free (« *fully free* ») boundary conditions

$$\text{I}: \ \partial_z\psi = 0\,, \ \partial_z v_y = 0\,, \ \partial_z^2 v_z = 0\,, \ z = \pm \pi/2\,. \tag{2.20a}$$

The last equation is equivalent to $\partial_z v_x = 0$ when equation (2.14) and the other boundary conditions are taken into account. For most situations the case of *fully rigid* boundary conditions is quite realistic

$$\text{II}: \ \psi = 0\,, \ v_y = 0\,, \ \partial_z v_z = 0\,, \ z = \pm \pi/2\,. \tag{2.20b}$$

The last equation is equivalent to $v_x = 0$. Under some conditions the combination of *torque-free* and *velocity-rigid* boundary conditions

$$\text{III}: \ \partial_z\psi = 0\,, \ v_y = 0\,, \ \partial_z v_z = 0\,, \ z = \pm \pi/2 \tag{2.20c}$$

appear relevant. The opposite combination does not seem important, but will be discussed occasionally later on. In equations (2.20a) and in (2.20b), (2.20c) it is assumed that the anchoring against twist deformations at the surface is weak and strong, respectively, compared to the destabilizing torques.

3. Linear analysis.

We consider a situation with the undistorted director $\hat{n}$ in the x-direction, applied voltage $V(t) = \sqrt{2}\bar{E}d \cos \omega t = \sqrt{2}\bar{V} \cos \omega t$ ($\bar{V}$ = effective voltage) between the plates (see Fig. 1) and an applied

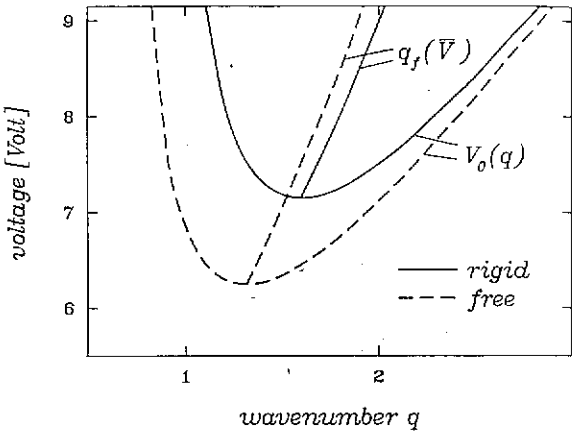

Fig. 2. — The neutral curve $V_0(q, p = 0)$ and the wavenumber $q_f(\bar{V})$ corresponding to the maximum growth rate above threshold are shown for free (dashed line) and rigid boundary conditions (solid line) at the external frequency $\omega\tau_0 = 0.5$. The physical wavenumber is obtained by multiplying q by π/d. The material parameters for MBBA I (see Appendix D) have been used.

magnetic field H_i in the direction of one of the coordinate axes. In this section the general analysis leading to the determination of the threshold for instability of the rest state is presented. Thus the quantities ϕ, θ, ψ, v_x, v_y, v_z are assumed small. No further assumption about the spatial structure is made, and therefore a full 3-dimensional analysis is necessary.

3.1 THE LINEARIZED EQUATIONS. — From translational invariance in the x-y-plane follows that the linear modes are harmonics in x and y. Since the magnetic field is along one of the coordinate axes there is also reflexion symmetry in x and y and the following Ansatz is convenient

$$\begin{aligned} \theta &= \tilde{\theta}(z, t) \cos(qx + py)\,, \\ \psi &= \tilde{\psi}(z, t) \sin(qx + py)\,, \\ \phi &= \tilde{\phi}(z; t) \sin(qx + py) \\ v_{x/y} &= \tilde{v}_{x/y}(z, t) \cos(qx + py)\,, \\ v_z &= \tilde{v}_z(z, t) \sin(qx + py) \end{aligned} \tag{3.1}$$

(tildes are omitted in the following) and one arrives at

$$[-\varepsilon_0(\varepsilon_\parallel q^2+\varepsilon_\perp p^2)\,\partial_t-(\sigma_\parallel q^2+\sigma_\perp p^2)+(\sigma_\perp+\varepsilon_0\,\varepsilon_\perp\,\partial_t)\,\partial_z^2]\times$$
$$\times\phi+\frac{\sqrt{2}}{\pi}\bar{V}\,e^{i\omega t}[\sigma_a+\varepsilon_0\,\varepsilon_a(i\omega+\partial_t)]\,q\theta+\text{cc}=0\,, \tag{3.2a}$$

$$\varepsilon_0\,\varepsilon_a\frac{\sqrt{2}}{\pi}\bar{V}\,e^{i\omega t}\,q\phi+\left[\gamma_1\frac{d^2}{\pi^2}\partial_t+L_2-\varepsilon_0\,\varepsilon_a\frac{1}{\pi^2}\bar{V}^2(1+e^{2i\omega t})-k_{11}\,\partial_z^2\right]\times$$
$$\times\theta-(k_{11}-k_{22})\,p\,\partial_z\psi+\alpha_3\,\partial_z v_x+\alpha_2\,qv_z+\text{cc}=0\,, \tag{3.2b}$$

$$(k_{11}-k_{22})\,p\,\partial_z\theta+\left[\gamma_1\frac{d^2}{\pi^2}\partial_t+L_1-k_{22}\,\partial_z^2\right]\psi-\alpha_3\,pv_x-\alpha_2\,qv_y+\text{cc}=0\,, \tag{3.2c}$$

$$-\alpha_3\,p\frac{d^2}{\pi^2}\partial_t\,\partial_z\,\theta+(\alpha_2\,q^2-\alpha_3\,p^2)\frac{d^2}{\pi^2}\partial_t\psi+\left[\rho_m\frac{d^2}{\pi^2}\partial_t+(\eta_0-\eta_1-\alpha_2)\,q^2+\eta_2\,p^2-\eta_2\,\partial_z^2\right]pv_x+$$
$$+\left[-\rho_m\frac{d^2}{\pi^2}\partial_t+(\eta_2-\alpha_3-\alpha_4)\,p^2-\eta_1\,q^2+\frac{\alpha_4}{2}\partial_z^2\right]qv_y-qp\left(\eta_2-\alpha_3-\frac{\alpha_4}{2}\right)\partial_z v_z+\text{cc}=0 \tag{3.2d}$$

$$\frac{\sqrt{2}}{\pi}\bar{V}\,e^{i\omega t}[\varepsilon_\parallel q^2+\varepsilon_\perp p^2-\varepsilon_\perp\,\partial_z^2]\,\varepsilon_0\,q\phi-\left[(\alpha_2\,q^2+\alpha_3\,\partial_z^2)\frac{d^2}{\pi^2}\partial_t+\varepsilon_0\,\varepsilon_a\frac{1}{\pi^2}\bar{V}^2\,q^2(1+e^{2i\omega t})\right]\theta-$$
$$-\alpha_3\,p\frac{d^2}{\pi^2}\partial_t\,\partial_z\psi+\left[\rho_m\frac{d^2}{\pi^2}\partial_t+(\eta_0-\alpha_2-\eta_1)\,q^2+\eta_2\,p^2-\eta_2\,\partial_z^2\right]\partial_z v_x$$
$$+qp\left(\eta_2-\alpha_3-\frac{\alpha_4}{2}\right)\partial_z v_y-\left[\rho_m\frac{d^2}{\pi^2}+\eta_1\,q^2+(\eta_2-\alpha_3-\alpha_4)\,\partial_z^2+\frac{\alpha_4}{2}p^2\right]qv_z+\text{cc}=0 \tag{3.2e}$$

$$-qv_x-pv_y+\partial_z v_z=0 \tag{3.2f}$$

(cc = complex conjugate) where the following abbreviations were introduced

$$\begin{aligned}L_1&=k_{11}\,p^2+k_{33}\,q^2+h_x^2-h_y^2\,,\\ L_2&=k_{22}\,p^2+k_{33}\,q^2+h_x^2-h_z^2\,.\end{aligned} \tag{3.3}$$

The shear viscosities

$$\begin{aligned}\eta_1&=(\alpha_4+\alpha_5-\alpha_2)/2\\ \eta_2&=(\alpha_3+\alpha_4+\alpha_6)/2\\ \eta_0&=\alpha_1+\alpha_4+\alpha_5+\alpha_6\end{aligned} \tag{3.4}$$

are defined as usual [1] and

$$h_i=\sqrt{\chi_a\,\mu_0}H_i\,d/\pi=k_{11}\,H_i/H_F\,. \tag{3.5}$$

(H_F = splay-Fréedericksz-transition field). We remind that only one of the components H_i is allowed to be nonzero.

The system of equations can be written in matrix notation in the form

$$\mathbf{B}\,\partial_t\mathbf{u}=\mathbf{L}\mathbf{u} \tag{3.6}$$

where **B** and **L** are linear matrix-differential operators (differentiation with respect to z) and $\mathbf{u}(z,t)=(\phi,\ \theta,\ \psi,\ v_x,\ v_y,\ v_z)$. **B** and **L** depend (parametrically) on t and are in fact $2\pi/\omega$-periodic. From Floquet theory (see e.g. Ref. [30]) one therefore knows that the solutions of (3.6) can be expressed in the form

$$\mathbf{u}(z,t)=e^{\sigma t}\sum_n\mathbf{u}_n(z)\,e^{in\omega t} \tag{3.7}$$

where σ is the Floquet exponent, which we assume real (unless stated otherwise) and which plays the role of the growth rate. The reality condition gives $u_{-n}=u_n^*$. Substituting (3.7) into the system (3.2) shows that the odd Fourier coefficients of the induced potential ϕ do not couple to the even Fourier coefficients of the other components, and vice versa. Therefore one has two classes of solutions which are, respectively, relevant in the low-frequency « conduction » and high-frequency « dielectric » regime [31-34]. In the conduction regime at threshold we thus have

$$\begin{aligned}\phi(z,t)&=e^{\sigma t}\sum_n\phi_n(z)\,e^{i(2n+1)\omega t}\,,\quad \phi_{-(n+1)}=\phi_n^*\\ u(z,t)&=e^{\sigma t}\sum_n u_n(z)\,e^{i2n\omega t}\,,\qquad\qquad u_{-n}=u_n^*\end{aligned} \tag{3.8}$$

where now $u=\theta,\ \psi,\ v_y,\ v_x$ or y_z.

In general the set of equations (3.2) together with the boundary conditions (2.18)-(2.20) and the expansion (3.7), (3.8) have to be solved numerically to find the growth rate $\sigma(p,\ q\,;\ \bar{V},\ \omega)$ and from

$\sigma = 0$ the neutral surface $\bar{V} = V_0(q, p\,;\,\omega)$ for a steady bifurcation. Maximizing σ and minimizing V_0 with respect to q and p provide the fastest growing rate $\sigma_f(\bar{V}, \omega)$ and the absolute threshold $V_c(\omega)$ together with the corresponding wavevectors $\mathbf{q}_f = (q_f, p_f)$ and $\mathbf{q}_c = (q_c, p_c)$.

There exist, however, simplifying cases where analytic progress is possible. The most important one will be considered in the next subsection. There the z-dependence is eliminated by using appropriate analytic functions and the Fourier expansion in time is confined to the lowest-order terms. In Appendix C a scheme for keeping an arbitrary number of Fourier terms is introduced.

3.2 ANALYTIC THRESHOLD FORMULA. — Equations (3.2) as well as the fully free boundary conditions (2.18)-(2.20a) are satisfied by choosing

$$\begin{aligned} \phi_n(z) &= A_n \cos z\,, \quad \theta_n(z) = B_n \cos z\,, \\ \psi_n(z) &= C_n \sin z\,, \quad v_{zn}(z) = F_n \cos z\,, \\ v_{xn}(z) &= D_n \sin z\,, \quad v_{yn}(z) = E_n \sin z\,. \end{aligned} \tag{3.9}$$

In principle one could choose for the z-dependence higher harmonics but they lead to a higher threshold [35]. To obtain an analytical expression for the threshold voltage only the lowest components $n = 0$ in the Fourier expansion equation (3.8) are kept. This corresponds to the assumption that the electric quantities ϕ and ρ_c follow the external field essentially instantaneously whereas the director and velocity are essentially time independent. This is roughly justified if $\tau_d\,\omega \gg 1$ and $\tau_d \gg \tau_0$ ($\tau_d \sim \gamma_1 d^2/k_{11}$ = director relaxation time, $\tau_0 \sim \varepsilon_0\,\varepsilon_\perp/\sigma_\perp$ = charge relaxation time). The validity of the approximation as well as corrections to it are discussed in more detail later in subsection 4.3 (see also Ref. [34]).

With these specifications equations (3.2) become fully algebraic. Their final form is obtained by the following replacements :

$$\partial_z \to \begin{cases} 1 \text{ when acting on } \psi, v_x, v_y \\ -1 \text{ when acting on } \phi, \theta, v_z \end{cases}; \quad \partial_z^2 \to -1$$

$$\partial_t \to \begin{cases} i\omega \text{ when acting on } \phi \\ 0 \text{ otherwise} \end{cases}; \quad e^{i\omega t} \to 1,\ e^{2i\omega t} \to 0\,. \tag{3.10}$$

Also the cc can be omitted everywhere when ϕ is replaced by $1/2(\phi + \phi^*)$ in equations (3.2b) and (3.2e). The resulting set of homogeneous linear equations yields a determinantal condition which gives the following expression for the threshold of the effective voltage $V_0 = \bar{E}_0\,d$:

$$V_0^2 = \frac{\pi^2(1+\omega^2\tau^2)[K_2 - p^2(k_{11}-k_{22})^2\,I_2\,I_4/K_1]}{\varepsilon_a\,\varepsilon_0[q^2\,GM + D_1^{-1}(q^2+p^2+I_1)(D_1\,S^{-1}+\omega^2\tau^2)]} \tag{3.11}$$

where

$$K_1 = L_1 + k_{22}\,I_6\,; \qquad K_2 = L_2 + k_{11}\,I_1 \tag{3.12}$$

$$S = q^2\sigma_\parallel/\sigma_\perp + p^2 + I_1\,; \quad D_1 = q^2\varepsilon_\parallel/\varepsilon_\perp + p^2 + I_1$$

$$D_2 = (q^2\varepsilon_\parallel/\varepsilon_\perp + p^2)\,I_8 + I_9\,; \qquad G = \sigma_a\,\varepsilon_\perp\,D_1/(\sigma_\perp\,\varepsilon_a\,S) - 1 + \omega^2\tau^2(D_2/D_1 - 1)$$

$$\tau = \tau_0\,D_1/S\,; \quad \tau_0 = \varepsilon_0\,\varepsilon_\perp/\sigma_\perp \tag{3.13}$$

$$M = \{p^2[(\alpha_3 p^2 - \alpha_2 q^2)\,\beta_1 - \alpha_3\,\beta_2\,I_6](k_{11}-k_{22})\,I_2/K_1 + (\alpha_3\,I_2\,I_6 - \alpha_2\,I_3\,q^2)\,\beta_2 - \alpha_3\,\beta_1\,I_2\,p^2\}/(\beta_2\,\beta_3 - p^2\,\beta_1\,\beta_1') \tag{3.14}$$

$$\beta_1 = \left[\delta - \frac{1}{2}\alpha_4 q^2 + \eta_2 I_5\right] I_6\,, \quad \beta_1' = \left(\delta - \frac{1}{2}\alpha_4 q^2\right) I_7 + \eta_2 I_{10}$$

$$\beta_2 = \left[\delta p^2 + \eta_1 q^4 + \left(\eta_2 p^2 + \frac{1}{2}\alpha_4 q^2\right) I_5\right]$$

$$\beta_3 = q^2\left(\frac{\alpha_4}{2}p^2 + \eta_1 q^2\right) + \eta_2 I_6 I_{10} - ((\eta_1 + \alpha_2 - \eta_0)\,q^2 - \eta_2 p^2)\,I_6 I_7 - (\eta_2 - \alpha_3 - \alpha_4)\,I_{11}\,q^2$$

$$\delta = (\eta_1 + \eta_2 + \alpha_1)\,q^2 + \eta_2 p^2$$

with $I_1 = \cdots = I_{11} = 1$. As shown in Appendix A the above threshold formula with $I_1, \ldots, I_{11}$ different from 1 can be obtained as an approximation to the problem for the other boundary conditions by a Galerkin procedure with simple trial functions. This approximation will be used again in subsection 4.3.

The expression (3.11) includes all well-known limiting cases : for $q^2 \gg 1$ and $p = 0$ the one-dimen-

sional description of the Williams domains, which has been used extensively, is obtained [36, 32]. For $p = 0$ and $I_i = 1$ the result for the two-dimensional analysis for free boundary conditions is recovered [37]. For $q = 0$ the recently discovered periodic splay-twist instability is described [14] (see also Subsect. 4.4). Setting $\omega = 0$ in equation (3.11) gives the threshold for an applied dc voltage.

We emphasize that according to equation (3.11) the voltage threshold is independent of thickness d. This result is exact in the time-independent case. As can be seen from equation (3.2) the thickness appears explicitly, even in the conduction regime, when higher-order terms in the time-Fourier expansion (3.8) are included (see Appendix C).

4. Results of the linear analysis.

In this section we present our results for the two-dimensional neutral surface $V_0(q, p; \omega)$ and its minimum $V_c(\omega)$ with respect to $\mathbf{q} = (q, p)$ giving the critical wavevector $\mathbf{q}_c(\omega)$. Some results on the fastest-growing modes $\mathbf{q}_f(\bar{V}, \omega)$ above threshold are also given. V_c gives the absolute threshold for the instability as long as the bifurcation to the new state is steady and supercritical (or forward) leading to a continuous, reversible transition. If the system is driven slowly across threshold the critical wavenumber $\mathbf{q}_c$ first established should be maintained even above threshold under appropriate conditions (i.e. no secondary transitions, no wavelength-changing processes initiated by instabilities — see e.g. Ref. [38] and references cited therein —, or by finite fluctuations or perturbations). If, on the other hand, a sudden jump to a supercritical state $\bar{V}$, ω is imposed the fastest-growing mode $\mathbf{q}_f$ should be favored under similar ideal conditions. This type of hysteretic behavior is characteristic for macroscopic pattern-forming systems and will be discussed in greater detail in the next section.

The following presentation is subdivided into four subsections: first we consider normal rolls ($p = 0$) and then oblique rolls, both in the lowest-order time-Fourier approximation for free and (rigorous) rigid boundary conditions (Subsect. 4.1 and 4.2). Next, the higher-order time-Fourier expansion, which is essentially a full solution in the time-variable, is presented in subsection 4.3. This is done only in connection with free boundary conditions and with trial functions that approximate rigid boundary conditions. The technical parts of the calculations are given in Appendix C in connection with Appendix A. Finally in subsection 4.4 we discuss the case $q = 0$, $p \neq 0$, which corresponds to the periodic splay-twist transition. In the actual computations of this section we mostly used material parameters of MBBA which were measured fairly recently and which are summarized in Appendix D (« MBBA I »). Some computations in this section and all in the next section were done with older parameter values also given in Appendix D (« MBBA II »). Actually the two parameter sets lead only to minor quantitative changes.

4.1 NORMAL ROLLS, LOWEST-ORDER FREQUENCY EXPANSION. — We first discuss the traditional case of normal rolls which is obtained by setting $p = 0$ in the equations of section 3 (two-dimensional description). In figure 2 the neutral curve $V_0(q)$ is shown for MBBA I (material parameters see Appendix D) at $\omega\tau_0 = 0.5$ for free (as calculated from Eq. (3.11)) as well as for (rigorous) rigid boundary conditions. Also included is the wavenumber $q_f(\bar{V})$ corresponding to maximum growth rate above threshold. In figure 3 the minimum V_c of the neutral curve and the

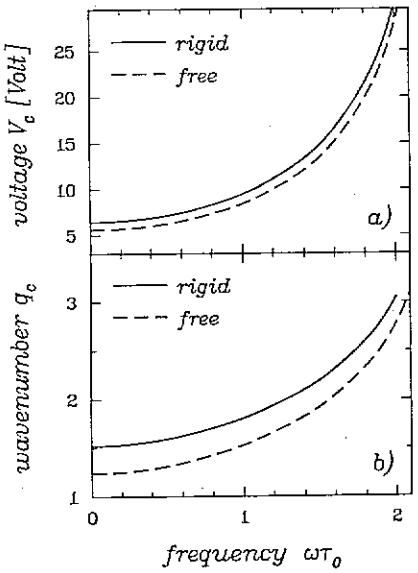

Fig. 3. — The voltage V_c (absolute threshold) and the critical wavenumber q_c (physical units: multiply by π/d) are shown as a function of the external frequency for free and rigid boundary conditions ($\tau_0 = \varepsilon_0 \varepsilon_\perp / \sigma_\perp$, material parameters for MBBA I).

critical wavenumber q_c is shown as a function of frequency for free and (rigorous) rigid boundary conditions. Going over to rigid boundary conditions mainly rescales the whole neutral curve to higher q and $\bar{V}$. This can be understood in terms of the boundary layers resulting from the friction at the upper and lower plates which reduce the effective thickness of the layer. With increasing frequency the width of the neutral curve decreases but the normalized curvature $(d^2 V_0(q)/dq^2)/V_c$ at q_c remains essentially constant. The same is true for V_c/q_c^2.

For $q^2 \gg 1$ equation (3.11) goes over into

$$V_0^2 = \frac{\pi^2(1 + \omega^2\tau^2)\, k_{33}\, \sigma_\parallel^2\, q^2}{\varepsilon_0^3\, \varepsilon_\parallel\, \varepsilon_\perp\, \varepsilon_a(\omega^2 - C)} \qquad (4.1)$$

so that V_0 increases linearly with q. Here

$$C = \frac{\sigma_\parallel}{\varepsilon_0^2 \varepsilon_\perp} \left[\frac{-\alpha_2}{\eta_1} \left(\frac{\sigma_\parallel}{\varepsilon_\parallel} - \frac{\sigma_a}{\varepsilon_a} \right) - \frac{\sigma_\perp}{\varepsilon_\parallel} \right] . \quad (4.2)$$

Since in this limit effects from the upper and lower plates become negligible equation (4.1) also holds for rigid boundary condition (it is even the same in the one-dimensional model [32]). For $\varepsilon_a < 0$ (negative dielectric anisotropy) the constant C is positive and then $\omega_c = \sqrt{C}$ is the so-called cut-off frequency. At ω_c both V_c and q_c diverge such that V_c/q_c^2 goes to a finite limit and above ω_c there is no EHC with the modes of the conductive regime. The reason for this is that build-up of space charges *via* the Carr-Helfrich mechanism which is governed by the charge relaxation time and which drives EHC (see e.g. [36, 32, 1, 13]) becomes less effective with increasing frequency, so that the destabilizing effects eventually cannot overcome the dielectric torques which are stabilizing for $\varepsilon_a < 0$.

For $\varepsilon_a < 0$ and all frequencies $\omega\ (< \omega_c)$ the neutral curve $V_0(q)$ diverges on the low-q side at a nonzero wavenumber q_{min}. Although with decreasing ε_a the stabilizing effects become stronger and q_{min} increases there is no critical value below which EHC does not occur at all. A conclusion to the contrary was reached previously in the context of the one-dimensional model [32, 1]. This conclusion depends on the assumption that the critical wavenumber remains of order 1 (or π/d in physical units), which is in fact incorrect.

For $\varepsilon_a > 0$ the neutral curve $V_0(q)$ tends to a finite value for $q \to 0$ and $V_0(0) = V_F = (\pi^2 k_{11}/\varepsilon_0 \varepsilon_a)^{1/2}$ then corresponds to the threshold of the spatially homogeneous splay Fréedericksz transition. Varying ε_a and leaving all other parameters fixed leads to a critical value ε_{ac} of ε_a below which EHC has a lower threshold than the Fréedericksz transition whereas for $\varepsilon_a > \varepsilon_{ac}$ the reverse is true. For MBBA I at $\omega = 0$ one has $\varepsilon_{ac} = 0.29$ and 0.56 for rigid and free boundary conditions, respectively. An additional magnetic field H_z in the z-direction lowers the threshold of the Fréedericksz transition more effectively than the threshold of the convective transition. Thus for $0 < \varepsilon_a < \varepsilon_{ac}$ and a definite value $H_z(\varepsilon_a)$ the thresholds become equal. Usually the neutral curve $V_0(q)$ has minima at $q = 0$ and $q = q_c$ and a maximum in between. For free boundary conditions this is easily seen by expanding the expression (3.11) for small $q^2(p = 0)$:

$$V_0^2/V_F^2 = 1 + \left\{ \frac{k_3}{k_{11}} - 1 + \left[\frac{\sigma_\parallel}{\sigma_\perp} - 1 + \right.\right.$$
$$\left.\left. + \omega^2 \tau_0^2 \frac{\varepsilon_\parallel}{\varepsilon_\perp} + \frac{\alpha_3}{\eta_2} \left(1 - \frac{\sigma_a \varepsilon_\perp}{\sigma_\perp \varepsilon_a} \right) \right] / (1 + \omega^2 \tau_0^2) \right\} q^2 . \quad (4.3)$$

The term in curly brackets is positive for all materials we know of. The fact that the threshold for EHC increases with increasing frequency can also be used to reverse the order of the transitions and this is shown for MBBA I in figure 4. The situation where the two thresholds are equal is of special interest. It represents one type of a so-called codimension-2 bifurcation [39]. This situation is similar to that found in the shear-flow instabilities in nematics [40]. For increasing H_z of ω the critical wavenumber q_c first increases and then decreases down to values $q_c \sim 0.6 - 1.2$ at the codimension-2 point.

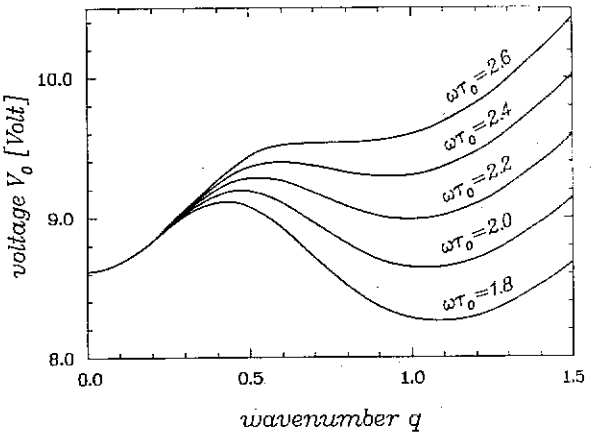

Fig. 4. — The neutral curve $V_0(q, p = 0)$ is shown for different reduced external frequencies $\omega\tau_0$ and rigid boundary conditions. The material parameters for MBBA I have been used, but ε_a was changed to 0.1 in order to exhibit the possibility of equal thresholds for the two instabilities.

Applying a magnetic field H_x in the x-direction stabilizes the undistorted orientation ($\chi_a > 0$) and also makes the surface anchoring less important. The threshold for EHC as well as the critical wavenumber q_c increase in agreement with the observations [42] (see also Fig. 11).

4.2 OBLIQUE ROLLS, LOWEST-ORDER FREQUENCY EXPANSION. — A necessary condition for the normal-roll threshold discussed above to be the absolute threshold is that $\partial^2 V_0(q, p)/\partial p^2 > 0$ at $q = q_c$ and $p = 0$. Otherwise there exists a lower threshold at $|p| = p_c > 0$ (oblique rolls). In figure 5 we have plotted V_0 and $\partial^2 V_0/\partial p^2$ as a function of q at $p = 0$ and $\omega = 0$ for MBBA I ($\varepsilon_a = -0.53$) and free boundary conditions. Although in this case normal rolls have the lowest threshold ($\partial^2 V_0/\partial p^2$ slightly positive at q_c) the plot demonstrates a very general feature: whereas for large q one always has $\partial^2 V_0/\partial p^2 > 0$, there is generally a value q_n at which $\partial^2 V_0/\partial p^2$ changes sign. By changing the material parameters one easily finds situations with $q_n > q_c$ at low frequencies ω. Most effective is a change of

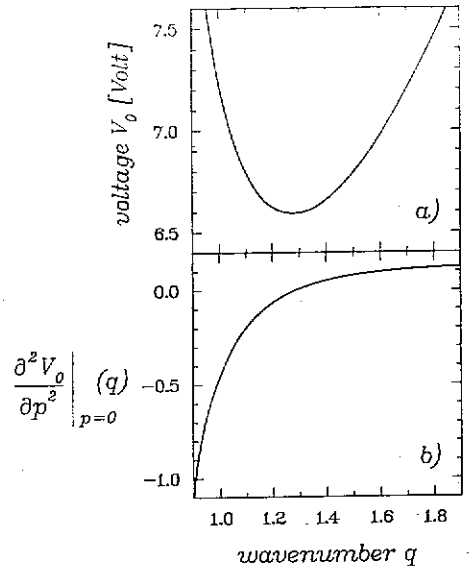

Fig. 5. — The neutral curve $V_0(q, p = 0)$ and the curvature $(\partial^2 V_0/\partial p^2)(q, p = 0)$ are shown for material parameters of MBBA I. This illustrates that for smaller values of q oblique rolls are favored.

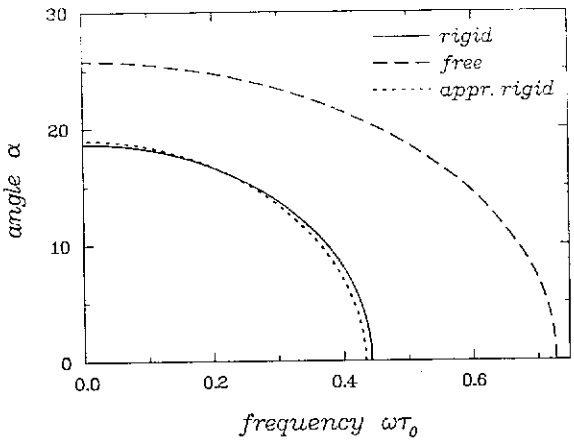

Fig. 6. — The roll angle $\alpha_s = \arctan(p_c/q_c)$ with respect to the y-axis is shown for rigid (solid line) and free boundary conditions (dashed line) as well as for the approximate rigid boundary conditions (dashed-dotted line) (Eq. (3.11) with I_i from Appendix A). Material parameters for MBBA I with modified conductivity $\sigma_\parallel/\sigma_\perp = 2.0$.

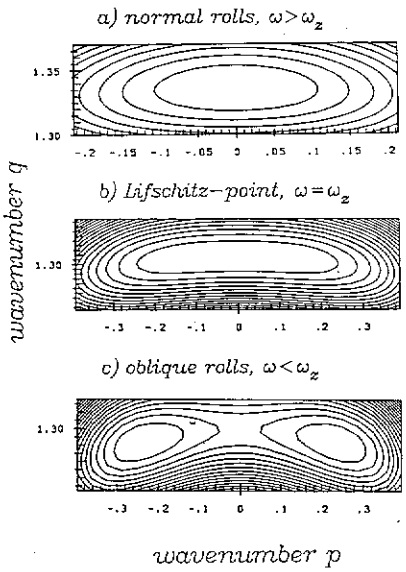

Fig. 7. — The contour lines of the neutral surface $V_0(q, p\,;\,\omega)$ are plotted for the frequencies $\omega > \omega_z$ (a), $\omega = \omega_z$(b), and $\omega < \omega_z$ (c). Material parameters of MBBA II and the modified ratio $\sigma_\parallel/\sigma_\perp = 2.0$ and $\varepsilon_a = -0.2$ and rigid boundary conditions.

ε_a to values above about -0.1 (for rigid boundary conditions) or $\sigma_\parallel/\sigma_\perp$ from the standard value 1.5 to 1.77 (for rigid boundary conditions). With increasing frequency $q_n - q_c$ always decreases and changes sign at some value ω_z.

In the cases that we have studied the quantity $\partial^4 V_0/\partial p^4$ is always positive so that p_c increases smoothly from 0 when the normal-oblique transition at ω_z, where $q_n - q_c$ becomes positive, is crossed. This transition was observed experimentally by crossing the neutral curve by increasing $\bar{V}$ at fixed frequency ω, and repeating the process at a sequence of decreasing frequencies, in a material where one has oblique rolls for small ω [5, 6]. Such a transition is described by the theory. In figure 6 the frequency-dependence of the roll angle $\alpha_s = \arctan(p_c/q_c)$ is shown for MBBA I with $\sigma_\parallel/\sigma_\perp = 2$ (free and rigid boundary conditions). At ω_z there is the typical pitchfork bifurcation which we always find for the transition to the oblique-roll state. The divergence of the slope of $p_c(\omega)$ at ω_c has apparently not been observed [5, 6]. Figure 6 exhibits the general tendency of rigid boundary conditions to suppress oblique rolls. Also included in figure 6 (dotted line) are the results from the approximate rigid boundary conditions as obtained from the analytical formula (3.11) with the I_i given in Appendix A. In figure 7 the contour lines of the neutral surface $V_0(q, p)$ are shown for three different frequencies : $\omega > \omega_z$ (normal rolls), $\omega = \omega_z$ (« Lifshitz-point », see Sect. 5) and $\omega < \omega_z$ (oblique rolls). One can see that at the minima the curvature in the p-direction is much smaller than that in the q-direction. The two curvatures become nearly equal for frequencies above about 50 % of the cut-off frequency (see also Figs. 15b and 17b). By using material parameters for PAA (see e.g. Ref. [41]) our calculations show that for rigid boundary conditions oblique rolls have the lowest absolute threshold in a large frequency range $0 < \omega\tau_0 < 1.31$. In the early experiments done by Williams [43] and later by Penz [44] oblique rolls seem actually to have been observed in PAA.

The angle $\alpha_v = \arctan(v_y/v_x)$ of the motion of the fluid projected onto the x-y-plane is different

from α_s, so that the fluid does not move perpendicular to the rolls. For the parameters of MBBA II and the modified values $\varepsilon_a = -0.2$ and $\sigma_\parallel/\sigma_\perp = 2.0$ we find $\alpha_v/\alpha_s \approx 0.78$ for free boundary conditions (independent of z and weakly dependent on ω). For rigid boundary conditions the maximum of α_v/α_s is about 0.23 (again weakly dependent on ω). We note that due to the $\pm z$-symmetry the fluid particles move on closed trajectories.

In principle the value of ω_z depends on all material parameters. In figure 8 we show the very sensitive dependence of ω_z on ε_a (Fig. 8a) and $\sigma_\parallel/\sigma_\perp$ (Fig. 8b). In Figure 8b the case of torque-free and velocity-rigid boundary conditions (Eq. (2.20c)) is included in order to demonstrate the general feature that this case is seen to lie between the fully free and rigid cases. A detailed study of the dependence of ω_z on small changes of parameters for an MBBA-like material was published previously for free boundary conditions (see Tab. I in Ref. [13]). We have repeated this study with rigid boundary conditions and generally found the same tendencies. The only exceptions are α_3 and α_5 which must be varied in the opposite direction to favor oblique rolls (the dependence of V_c and q_c remains the same).

Of course ω_z is also influenced by a magnetic field applied along one of the coordinate axes. A magnetic field in the x-direction increases V_c and q_c (see Sect. (4.1)). For free and torque-free boundary conditions it suppresses or favors oblique rolls, depending on the chosen parameters, whereas for rigid boundaries it generally favors them. A magnetic field in the z-direction decreases V_c and q_c. For free boundary conditions the oblique rolls are favored whereas for the other two boundary conditions they are suppressed. A magnetic field in the y-direction can only be used for rigid boundary conditions since for the other cases the critical field for the twist-Fréedericksz transition is zero. Application of the field favors oblique rolls. The changes that can be produced by H_y and H_z are small because the fields are limited by the Fréedericksz transition.

Finally we point out that for $\varepsilon_a > 0$ one can have competition between the oblique-roll state and the homogeneous splay Fréedericksz transition. The situation then is analogous to the one discussed in subsection 4.1 for normal rolls.

It is not easy to understand all the trends in terms of simple physical ideas because of the combination of antagonistic effects. A direct manifestation of this is shown by the fact that q_c and q_n (see Fig. 5) have to be affected in opposite directions to favor oblique rolls. It is easy to see that the basic Carr-Helfrich mechanism that drives EHC also provides the driving force for oblique rolls. A fairly detailed discussion is given elsewhere [13, 45].

We conclude this section by giving some results on the fastest-growing modes above threshold for free boundary conditions. In figure 9 the p-dependence

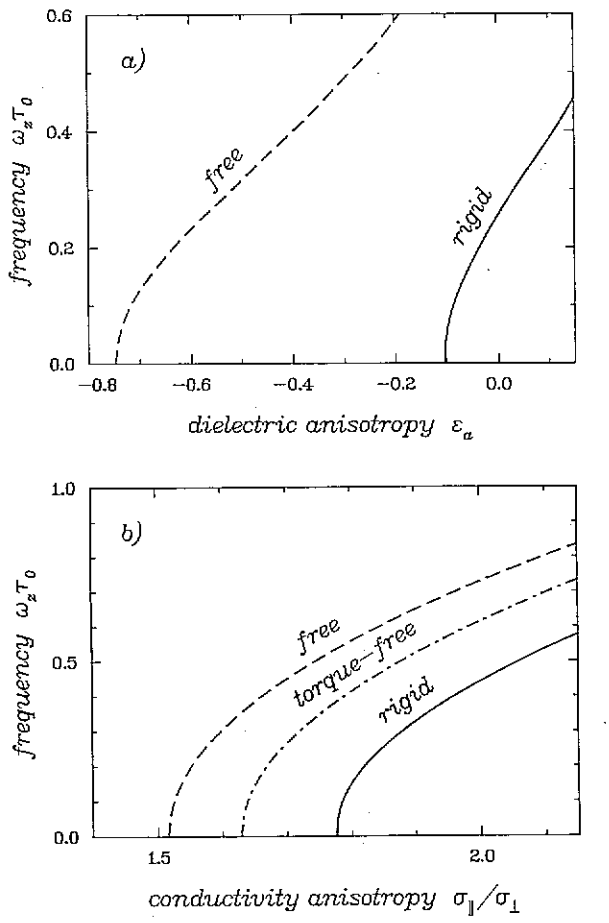

Fig. 8. — The reduced frequency $\omega_z \tau_0$, which limits the range of oblique rolls from above, is plotted as a function of the anisotropies ε_a (a), and $\sigma_\parallel/\sigma_\perp$ (b) for different boundary conditions. Material parameters for MBBA I and $\bar{\varepsilon} = (2\varepsilon_\perp + \varepsilon_\parallel) = 15.22$ are used.

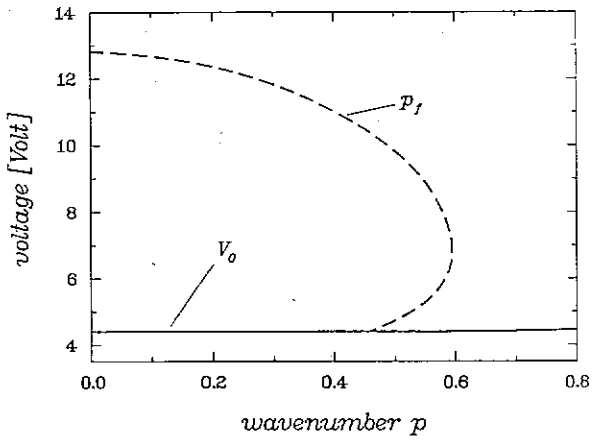

Fig. 9. — The neutral curve $V_0(p)$ (solid line) and wavenumber $p_f(\bar{V})$ (dashed line) corresponding to the maximum growth rate above threshold is shown for free boundary conditions and constant wavenumber $q = q_c$. Material parameters for MBBA I with modified values $\varepsilon_a = -0.2$ and $\sigma_\parallel/\sigma_\perp = 1.7$ are used.

of the neutral surface, i.e. $V_0(q_c, p)$, is shown for $\omega = 0$ (solid curve). It has a very small positive curvature. The dashed curve gives the fastest growing wavenumber p_f. In figure 10 the curves with constant angle $\alpha_f = \arctan(p_f/q_f)$ are plotted in the ω-$\bar{V}$-plane (solid curves) together with the threshold V_c (dashed curve). One sees that slightly above threshold oblique rolls (or larger angles) are favored somewhat, whereas higher up the trend reverses and eventually normal rolls are favored. This trend is similar to the behavior in transient spatial periodic patterns [46].

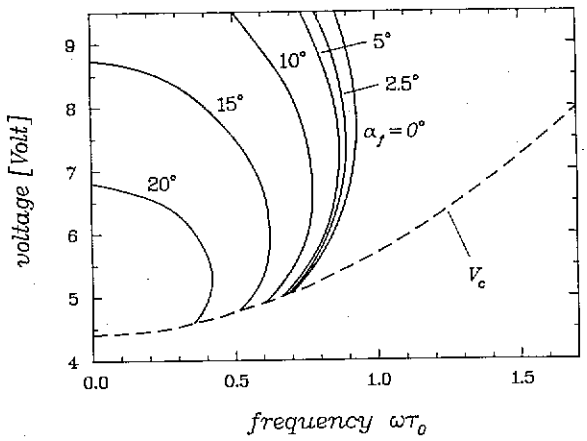

Fig. 10. — The threshold $V_c(\omega)$ (dashed line) and the contour lines $\alpha_f(\bar{V}, \omega) = \arctan(p_f/q_f) = 0°$, 2.5°, 5°, 10°, 15°, 20°. For given values $\bar{V}$ and ω the linear growth rate has its maximum at q_f, p_f. Free boundary conditions and material parameters for MBBA I with the modified parameters $\varepsilon_a = -0.2$ and $\sigma_1/\sigma_\perp = 1.7$ have been used.

4.3 HIGHER-ORDER TIME-FOURIER EXPANSION (« FULL THEORY »). — In the calculations of this subsection we treat the z-dependence only by trial functions which are exact for free boundary conditions and approximate for rigid boundary conditions, and which are introduced in subsection 3.2 in connection with Appendix A. The technical part of the calculations for this subsection are given in Appendix C.

Before presenting results of the more general calculations we discuss the range of validity of the lowest-order time-Fourier approximation (conduction regime) and the limit $\omega \to 0$. For the validity of the approximation the conditions that the director relaxation is slow compared to charge relaxation and to the external time-dependence imposed by the ac voltage is sufficient. The first condition can be written as

$$\tau_d = \left[\gamma_1 - \frac{(\alpha_2 q^2 - \alpha_3)^2}{\beta_3}\right] \frac{d^2}{\pi^2 K_2} \gg (1 + \bar{V}^2/R)\,\tau \tag{4.4}$$

where τ_d is the director relaxation time at $\bar{V} = 0$ (and $p = 0$), τ is the charge relaxation time, equation (3.13), and

$$R = -(\beta_3 K_2 \pi^2/\varepsilon_0 \varepsilon_a)/[\beta_3 + (\alpha_2 q^2 - \alpha_3) q^2]\,. \tag{4.5}$$

The second condition is simply

$$\tau_d \omega \gg 1\,. \tag{4.6}$$

For $q = p = 0$ and no magnetic field one has essentially $\tau_d = \gamma_1 d^2/k_{11}\pi^2$, $\tau = \tau_0$ and $R = -k_{11}\pi^2/\varepsilon_0\varepsilon_a$. The last expression for R coincides with $-V_F^2$ if $\varepsilon_a > 0$ (V_F = Fréedericksz transition voltage).

Actually our numerical results indicate that, as long as (4.4) holds, the neutral curve obtained in lowest-order time-Fourier approximation remains valid even for quite low frequencies where (4.6) is definitely violated. This would mean that, if (4.4) is valid, the ac threshold for $\omega \to 0$ coincides, at least approximately, with the dc threshold. This can indeed be understood by analysing in equations (3.2) the limit $\tau_d \omega \to 0$, which is done in Appendix B for normal rolls. The analysis shows that the corrections are of order τ/τ_d, which is small when (4.4) holds, and usually positive, so that one expects the threshold to increase slightly with decreasing frequency for $\tau_d \omega \lesssim 1$. This effect has presumably been observed [47].

We point out that in the limit $\tau_d \omega \ll 1$ one can still define a sharp threshold where the growth rate (Floquet exponent) becomes positive so that a pattern which is coherent over long times builds up. This threshold, however, might be difficult to observe because fluctuation-induced patterns may occur already when only the voltage peaks exceed the dc threshold. These patterns do not exhibit long-time coherence, but they prevent a determination of the actual threshold.

Relation (4.4) has the consequence that the lowest-order time-Fourier approximation always fails sufficiently near to the cut-off frequency where V_c becomes large. Here indeed the behavior changes qualitatively (see below). Even at low voltages, equation (4.4) is easily violated by choosing a sufficiently small thickness d and clean material (low conductivity) [see e.g. Ref. [1]]. For MBBA I at $q = 1$, $p = 0$, one has $\tau_d \approx 0.6 \cdot 10^{-3}\ (d/\mu\text{m})^2$ and $\tau \approx 0.4 \cdot 10^{-10}\ \text{s}/(\sigma_\perp\ \Omega\text{m})$, so that for a typical value $\sigma_\perp = 10^{-8}\,\Omega^{-1}\,\text{m}^{-1}$ (this value will be used subsequently, if not stated otherwise) one has $\tau_d = \tau$ at $d \approx 2.5\ \mu\text{m}$. τ_d is also decreased by applying a magnetic field H_x in the x-direction through the influence on K_2 (see Eqs. (3.3) and (3.12)).

In figure 11 the threshold (a) and the critical

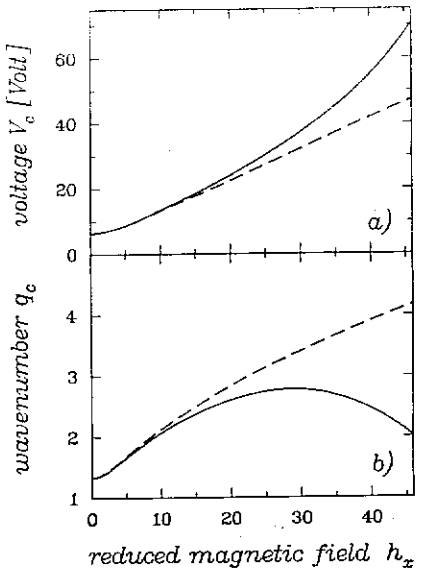

Fig. 11. — The threshold V_c (a), and the critical wavenumber q_c (b) are plotted at $p = 0$ and $\omega\tau_0 = 0.5$ for lowest-order time-Fourier approximation (dashed lines) and « full theory » as a function of the external magnetic field in x-direction $h_x^2 = \chi_a \mu_0 H_x^2 d^2/\pi^2 10^{12} \mathrm{N}^{-1} = 6.66 H_x^2/H_F^2$ (H_F = splay-Fréedericksz-transition field). Free boundary conditions and material parameters for MBBA I have been used.

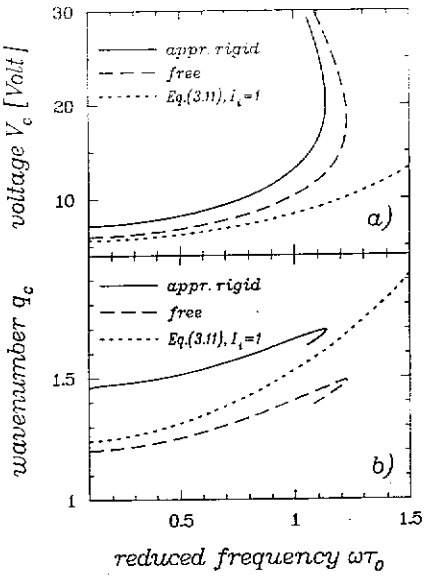

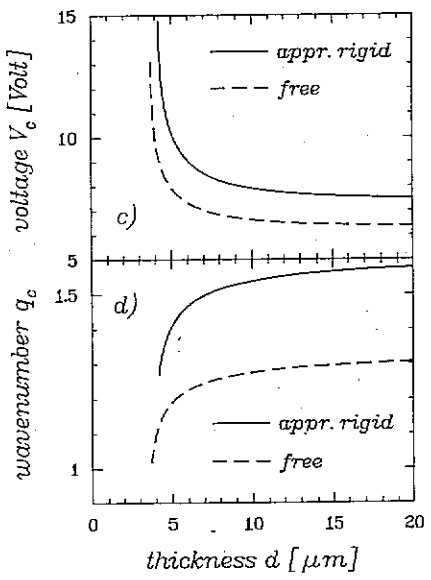

Fig. 12. — In a) and b) the threshold voltage V_c and the critical wavenumber q_c is plotted as function of the frequency $\omega\tau_0$ for the « full theory » at the thickness $d = 8$ μm (solid and dashed lines) and lowest-order time-Fourier expansion (dotted line : free b.c., i.e. Eq. (3.11) with $I_i = 1$). In c) and d) V_c and q_c are plotted as function of the thickness d at the frequency $\omega\tau_0 = 0.5$ for free and approximate rigid boundary conditions. Material parameters for MBBA I.

wavenumber q_c (b) are shown for free boundary conditions as a function of H_x for a layer of MBBA I with thickness $d = 50$ μm at $\omega\tau_0 = 0.5$. The difference between the broken curves (result for the lowest-order time-Fourier approximation) and the solid curves (« full theory », i.e. expansion to sufficient order) goes in parallel with the violation of equation (4.4). The increase of V_c is typical and well-known [42]. The decrease of q_c at higher fields indicates that there is a tendency towards oblique rolls, although in this case one still has normal rolls (see below). For rigid boundary conditions the results are qualitatively the same.

The effect of decreasing the thickness d is shown in figure 12 (MBBA I). In the limit $d \to \infty$, where the lowest-order time-Fourier approximation is exact (dotted curve in Figs. 12a and b, free boundary conditions), the conduction regime is limited from above by the cut-off frequency ω_c ($\omega_c \tau_0 \cong 2.53$ for MBBA I and free boundary conditions). For finite thickness (Fig. 12a and b, $d = 8$ μm) the threshold curve bends over leading to a maximum frequency ω_m above which the instability does not exist with the conduction mode [see e.g. 67-70, 48, 34, 1]. ω_m tends to ω_c for increasing thickness d. In the case of figure 12 one has $\omega_m \tau_0 = 1.13$ for approximate rigid and $\omega_m \tau_0 = 1.23$ for free boundary conditions. The decrease of the reduced wavenumber q_c (wavenumber in physical units = $q_c \pi/d$) by decreasing the thickness d can be seen from figure 12b for free boundary conditions by comparing the dashed and the dotted lines. For rigid boundary conditions the behavior is qualitatively the same. In figures 12c and 12d the increase of V_c and the decrease of q_c with decreasing thickness at fixed frequency $\omega\tau_0 = 0.5$ are shown. The curves end at low d when $\omega_m \tau_0$ reaches 0.5.

Actually for $\omega > \omega_m$ one has the well-known instability to the dielectric mode [1, 2], which we do

not consider here. The dielectric threshold curve crosses the restabilizing branch of the conduction mode. The restabilization is essentially due to the stabilizing dielectric torques, which exceed the destabilizing torques at high voltage. Therefore for more negative ε_a, restabilizing occurs at lower voltage. For a material with $\varepsilon_a = -5$ the restabilization was actually measured [48]. There, however, only normal rolls were found in agreement with our results.

For lowest-order time-Fourier approximation oblique rolls do not appear at any frequency for MBBA (I and II). By decreasing d we find with the full theory 3 typical scenarios for the position of the Lifshitz-point $\omega_z \tau_0$ which are demonstrated in figure 13 by using MBBA I with different conduction

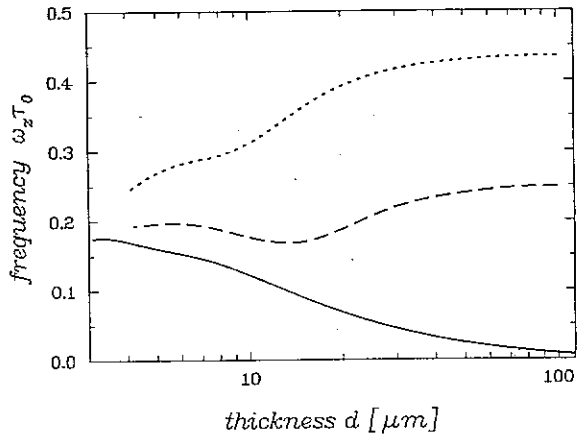

Fig. 13. — The position of the Lifshitz-point $\omega_z \tau_0$ is plotted as function of the sample thickness d for MBBA I with different conduction anisotropies $\sigma_\parallel/\sigma_\perp = 2.0$ (dotted line), $\sigma_\parallel/\sigma_\perp = 1.85$ (dashed) and $\sigma_\parallel/\sigma_\perp = 1.77$ (solid) for approximate rigid boundary conditions.

anisotropies : for $\sigma_\parallel/\sigma_\perp = 2.0$ one has in lowest-order time-Fourier approximation ($d \to \infty$) a Lifshitz-point at $\omega \tau_0 = 0.43$ which decreases for decreasing thickness d as shown by the dotted line in figure 13. For $\sigma_\parallel/\sigma_\perp = 1.77$ (and lower values of $\sigma_\parallel/\sigma_\perp$) there is no Lifshitz-point within the lowest-order time-Fourier approximation. By decreasing the thickness d a Lifshitz-point appears at low frequencies which increases up to $\omega_z \tau_0 = 0.176$ (solid line). This scenario is consistent with some experiments [47a]. Shortly before the conduction regime vanishes $\omega_z \tau_0$ decreases slightly. For an intermediate value $\sigma_\parallel/\sigma_\perp = 1.85$, $\omega_z \tau_0$ decreases at first for decreasing thickness d, then increases and decreases again before the conduction regime vanishes (dashed line). For standard MBBA I ($\sigma_\parallel/\sigma_\perp = 1.5$) an oblique-roll range appears to occur only at extremely low frequency ($\omega_z \tau_0 = 2.5 \times 10^{-3}$ at $d = 50$ μm). This point is not yet completely clear and will be investigated further.

By applying a stabilizing magnetic field H_x in x-direction a somewhat similar behavior of the Lifshitz-point $\omega_z \tau_0$ can be observed as in the case of decreasing the thickness. In figure 14 we have plot-

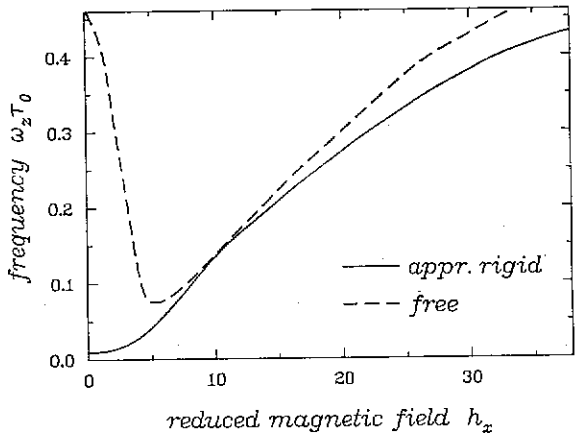

Fig. 14. — The position of the Lifshitz-point $\omega_z \tau_0$ as function of the external magnetic field $h_x^2 = \chi_a \mu_0 H_x^2 d^2/\pi^2 10^{12}\,\mathrm{N}^{-1}$ is plotted for free and approximate rigid boundary conditions. Material parameters of MMBA I with the modified ratio $\sigma_\parallel/\sigma_\perp = 1.72$.

ted $\omega_z \tau_0$ as a function of H_x for free and approximate rigid boundary conditions for MBBA I with $\sigma_\parallel/\sigma_\perp = 1.72$ at $d = 50$ μm. For approximate rigid boundary conditions $\omega_z \tau_0$ increased monotonically in all investigated cases, which appears consistent with experiment [47b], whereas for free boundary conditions both dependences on H_x were found. The same tendencies are obtained in the lowest-order time-Fourier approximation (see Subsect. 4.2).

As already remarked in section 4.2 it is not easy to understand all the trends in terms of simple physical ideas. It appears that the results on the oblique-roll behavior are usually the consequence of a complicated balance of antagonistic effects. A further complication is due to the fact that, when corrections to the lowest-order time-Fourier expansion become important, the influence of the flexoelectric effect can nolonger be neglected (see Sect 6).

4.4 THE PERIODIC SPLAY-TWIST (PST) TRANSITION. Recently, Lonberg and Meyer [14] discovered that in nematic materials with a ratio of the twist and splay elastic constants $r = k_{22}/k_{11}$ smaller than a critical value $r_c = 0.303$, the usual homogeneous splay Fréedericksz transition is replaced by a spatially periodic, static splay-twist distortion. This range of small r is important since it is often reached by mainchain polymer materials.

The distortions are periodic in the y-direction and

therefore correspond in our analysis to the case $q = 0$, $p \neq 0$. Then equation (3.11) reduces to

$$R_{z0}(p) = k_{11} I_1 + k_{22} p^2 + R_x - \frac{(k_{11} - k_{22})^2 I_4 I_7 p^2}{k_{11} p^2 + k_{22} I_6 + R_x - R_y} \quad (4.7)$$

where $R_i = V_i^2 \varepsilon_0 \varepsilon_a / \pi^2 + H_i^2 \mu_0 \chi_a d^2 / \pi^2$. Although in this formula electric and magnetic fields along any coordinate axis are allowed (including crossed electric and magnetic fields), the system should be driven across the instability by the field in the z-direction. As before one has $I_i = 1$ for free boundary conditions. For approximate rigid boundary conditions the I_i are given in Appendix A.

For $p = 0$ equation (4.7) describes the homogeneous Fréedericksz transition which can be driven magnetically ($\chi_a > 0$) or, for $\varepsilon_a > 0$, also electrically. A field in the x-direction is stabilizing ($R_x > 0$) except for the case of an electric field and $\varepsilon_a < 0$ ($R_x < 0$). Clearly the threshold can be lowered by having a finite wavenumber p if

$$I_4 I_7 (k_{11} - k_{22})^2 / k_{22} > k_{22} I_6 + R_x - R_y (> 0) \quad (4.8)$$

holds. Then one has the PST transition. For vanishing fields in the x- and y-direction the relation (4.8) becomes

$$r < r_c = 1/(1 + \sqrt{I_6/(I_4 I_7)}), \quad r = k_{22}/k_{11}$$

which reduces to $r_c = 0.5$ for free and $r_c = 0.298$ for the approximate rigid boundary conditions. This last value is close to the exact result $r_c = (\beta_0^2 + \beta_0)^{1/2} - \beta_0 = 0.303$ ($\beta_0 = 8/\pi^2 - 1$) [15, 17].

For stabilizing fields ($R_x - R_y > 0$) r_c is decreased and can be made arbitrarily small. Destabilizing fields ($R_x - R_y < 0$) have to remain below the threshold for the homogeneous twist-Fréedericksz transition. This threshold is zero for free boundary conditions and k_{22} for rigid boundary conditions. Thus, according to (4.8), in the latter case r_c can be increased to 0.329 (the exact value is 1/3 [14, 15]).

The critical wavenumber p_c is obtained by minimizing R_{z0} in equation (4.7) with respect to p. This yields $p_c = 0$ or

$$p_c^2 = \left\{ \left[\frac{(k_{11} - k_{22})^2}{k_{22}} I_4 I_7 (k_{22} I_6 + R_x - R_y) \right]^{1/2} - k_{22} I_6 - R_x + R_y \right\} / k_{11} \quad (4.9)$$

which is zero at $r = r_c$ (equality sign in (4.8)) and finite for $r < r_c$. Without fields in the x- and y-direction equation (4.9) reduces to

$$p_c^2 = \sqrt{I_4 I_6 I_7} (1 - r/r_c). \quad (4.10)$$

For $r = 0$ and rigid boundary conditions this gives $p_c = 1.3$, which should be compared to $p_c \approx 1.5$ from the rigorous analysis [14, 15]. For stabilizing fields ($R_x - R_y > 0$) p_c tends to infinity for $r \to 0$.

We conclude that the simple analytical formula (4.7), which is a special case of equation (3.11), gives a good semiquantitative description of the threshold scenario for the periodic splay-twist transition. In principle one can use the transition to determine k_{11} and k_{22}. This can be done even without a measurement of p_c if the threshold is measured as a function of R_x and is then compared with the theory. Alternatively, one might first measure k_{11} at values of R_x sufficiently large such that $p_c = 0$. Then a measurement of the value of R_x where p_c becomes finite, i.e., where the equality sign in (4.8) holds, leads to a determination of k_{22}.

In the electrically driven case the above results pertain to the dc case or to the ac case in lowest-order Fourier expansion. In this approximation all velocities are zero (no flow). Including higher Fourier modes shows that there is a small alternating flow proportional to $\omega \alpha_3 / \eta_2$ in the x-direction, i.e. along the stripes of the pattern. The changes of the neutral curve due to higher Fourier modes appear to favor the finite-p PST state, at least for not too low frequency. We plan to study these effects in more detail.

Finally we wish to discuss briefly the interplay of the PST transition and EHC as described by the full equation (3.11). When r is slightly below r_c, so that p_c is small, then there exist parameter ranges where the two-dimensional neutral surface has two minima, one with $q_c = 0$ (PST) and one with $q_c \neq 0$ (EHC). This situation is analogous to the competition of normal- or oblique-roll EHC with the homogeneous Fréedericksz transition discussed in subsections 4.1 and in 4.2. The relative heights of the two minima can again be adjusted by an additional magnetic field in the z-direction or by the frequency ω of the voltage. For larger values of p_c there exists only one minimum of the neutral surface. By varying the external parameters one can then go smoothly from EHC to PST.

5. Weakly nonlinear region.

In the vicinity of the threshold of a continuous (supercritical) bifurcation into the structured state the basic spatial periodic solutions and their slow modulations can be described by a complex amplitude (or envelope). This is well known for quasi-one-dimensional systems and for isotropic quasi-two-dimensional systems like Rayleigh-Bénard convection [49, 11]. The case of quasi-two-dimensional systems with axial anisotropy was discussed recently [8, 9]. Accordingly the complex envelope has to satisfy three different envelope equations, valid in

the normal-roll and oblique-roll regimes as well as in the vicinity of the Lifshitz point ($\omega = \omega_z$). Mean-flow effects are not included in this treatment [18, 19]. They are presently under investigation.

5.1 NORMAL-ROLL REGIME. — In the region where normal rolls appear at the absolute threshold of the electrohydrodynamic instability ($\omega > \omega_z$) and not too near to the Lifshitz point ($\omega = \omega_z$) the description of the physical quantities $\mathbf{u} = (\phi,\ \theta,\ \psi,\ v_x,\ v_y,\ v_z)$ close to threshold has the form

$$u_i(r, t) = \varepsilon^{1/2}[U_i\, A(X, Y, T)\, e^{iq_c x} + \text{cc}] \times \times \tilde{u}_i(z, t) + 0(\varepsilon)\,, \quad (5.1)$$

(see also Sect. 3.1). Here

$$\varepsilon = (V^2 - V_c^2)/V_c^2 \ll 1 \quad (5.2)$$

measures the distance from threshold V_c. The U_i are constants with $|U_i| = 1$, which can be chosen real for θ, v_x, v_y and imaginary for ϕ, ψ, v_z (see Eq. (3.1)). $A(X, Y, T)$ is the slowly varying envelope (on the scale of $2\pi/q_c$) with the slow variables chosen as

$$X = \varepsilon^{1/2} x\,,\ Y = \varepsilon^{1/2} y\,,\ T = \varepsilon t\,. \quad (5.3)$$

(X and Y have the same scaling because the neutral surface is parabolic in q and p). Then the envelope equation reads

$$T_0\, \partial_T A = [\xi_\parallel^2\, \partial_x^2 + \xi_\perp^2\, \partial_Y^2 + 1 - |A|^2]\, A\,. \quad (5.4)$$

Note that the parameters T_0, $\xi_\parallel$ and $\xi_\perp$ can all be scaled away from equation (5.4). The linear analysis of the previous sections provides these parameters as well as the functions $\tilde{u}_i(z, t)$ in equation (5.1) up to an overall normalization. This will be discussed presently.

The relaxation time T_0 is equal to $(d\sigma/d\varepsilon)^{-1}$ at $\varepsilon = 0$ and $q = q_c$, $p = p_c = 0$ (σ = linear growth rate, see Sect. 3.1). The longitudinal and transverse coherence lengths $\xi_\parallel$ and $\xi_\perp$ are determined from the curvatures of the neutral surface at $\varepsilon = 0$ and $q = q_c$, $p = p_c = 0$.

To see this we note that

$$A = F \exp[i(QX/\xi_\parallel + PY/\xi_\perp)] \times \times f(T)/[1 + f^2(T)]^{1/2}\,, \quad (5.5)$$

$$F = (1 - Q^2 - P^2)^{1/2}\,, \qquad f(T) = f_0 \exp(F^2\, T/T_0) \quad (5.6)$$

corresponds to roll solutions of equation (5.4) with wavenumbers

$$q = q_c + \varepsilon^{1/2}\, Q/\xi_\parallel\,,\ p = \varepsilon^{1/2}\, P/\xi_\perp\,. \quad (5.7)$$

and a time-dependent amplitude. Clearly for $Q^2 + P^2 < 1$ the rolls grow and become stationary for $T \to \infty$. Thus the neutral surface to lowest nontrivial order in ε is given by $Q^2 + P^2 = 1$, or

$$\varepsilon = \xi_\parallel^2 (q - q_c)^2 + \xi_\perp^2\, p^2\,. \quad (5.8)$$

Therefore $\xi_\parallel^2$ and $\xi_\perp^2$ are, respectively, the second derivatives of $\frac{1}{2} V_0^2/V_c^2$ with respect to q and p at q_c (and $p_c = 0$). From equations (5.5) and (5.6) one also sees that the fastest linear growth rate is T_0^{-1}, so that in physical units one has $\sigma = \varepsilon/T_0$ near threshold, or, as pointed out before, $d\sigma/d\varepsilon = T_0^{-1}$.

To determine the overall normalization of the $\tilde{u}_i$ one has to add to equations (3.2) the nonlinear terms up to third order in ϕ, θ, ψ, v_x, v_y, v_z. Then the q_c-periodic solution is expanded in the form

$$\mathbf{u} = \varepsilon^{1/2}[\mathbf{u}^{(0)} + \varepsilon^{1/2}\, \mathbf{u}^{(1)} + \varepsilon \mathbf{u}^{(2)} + \ldots] \quad (5.9)$$

where $\mathbf{u}^{(0)}$ corresponds to the linear approximation. Its normalization is determined by a solvability condition at order $\varepsilon^{3/2}$. The procedure is well-known in the analysis of the hydrodynamic instabilities of simple fluids [49, 11]. Unfortunately in our case it is very cumbersome due to the fact that the solutions at order ε are rather complex.

In our derivation we used the support of computer algebra (Macsyma) and calculated the equations for free and rigid boundaries for the conduction regime in the lowest-order Fourier expansion in time (see also Ref. [49a]). The final expressions are too complex to write down here, even in the case of fully free boundaries (except for T_0). In effect we have computer programs whose inputs are the parameters of the liquid crystal and the frequency of the electric field and the outputs are the quantities $u_i^{(0)}(z, t)$, T_0, $\xi_\parallel$ and $\xi_\perp$.

We also looked for dominant terms in the nonlinearities, but unfortunately without success. All contributions of the nonlinearities appear to have similar order-of-magnitude.

For $\omega \to \omega_z$, $\xi_\perp$ behaves as $\sqrt{\omega - \omega_z}$. In figure 15, T_0/d^2, $\xi_\parallel/d$ and $\xi_\perp/d$ are plotted as a function of $\omega\tau_0$ for fully rigid (solid curves) and fully free (dashed curves) boundary conditions (standard parameters of MBBA II, see Appendix D). In figure 16a, b the amplitudes of $\theta^{(0)}$, $v_x^{(0)}\, d$ and $v_z^{(0)}\, d$ at their respective maxima with respect to z are plotted as a function of $\omega\tau_0$ for fully rigid (solid curves) and fully free (dashed curves) boundary conditions for the same parameters. The amplitude I_{conv} of the external electric current carried by convection which can be expanded in ε is to order ε given in figure 16c. We have normalized it to the amplitude of the conductive current. The quantity

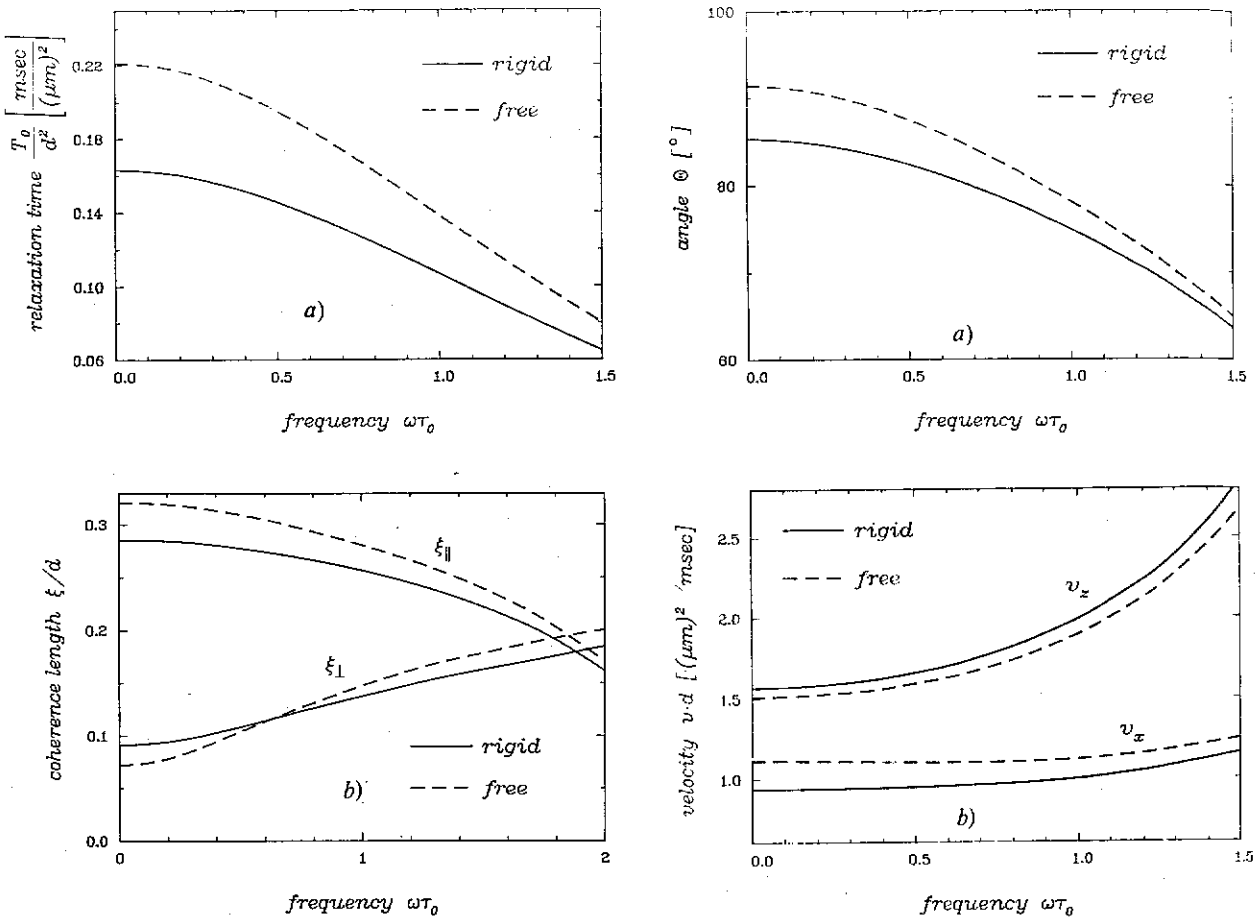

Fig. 15. — The relaxation time T_0 (a) and the coherence lengths $\xi_\parallel$ and $\xi_\perp$ (b) corresponding to equation (5.4) are plotted as a function of the reduced external frequency $\omega\tau_0$ for free and rigid boundary conditions. We have used units that exhibit the scaling with the layer thickness d and the conductivity $\sigma_\perp$ ($\tau_0 = \varepsilon_0 \varepsilon_\perp / \sigma_\perp$, material parameters for MBBA II).

Fig. 16. — The normalized amplitudes of the director distortion θ (a), the velocities v_x and v_y (b) and the convective current $I_{conv.}$ (c) are shown as a function of the reduced external frequency $\omega\tau_0$ for free and rigid boundary conditions. The physical values are obtained by multiplication with $\varepsilon^{1/2}$ (a, b) and ε (c) (material parameters for MBBA II).

may be termed « electric Nusselt number » in analogy to the corresponding quantity in Rayleigh-Bénard convection [50].

The quantities plotted exhibit the scaling properties with respect to changes of the thickness d. T_0 is of order of the director relaxation time τ_d, which scales like d^{-2}, and $v_i^{(0)}$ is of order d/τ_d. The magnitude of the conductivity $\sigma_\perp$ enters only through τ_0 (see Eq. (3.13)) into the scaling of ω. This behavior is strictly valid within the range of validity of the lowest-order time-Fourier expansion where the inequality (4.4) holds.

An estimate of the velocity by observing small glass spheres rotating with the fluid has been reported by Joets and Ribotta [6]. In the range $0.1 \lesssim \varepsilon \lesssim 0.5$ they find this velocity to be roughly proportional to ε ($v/\varepsilon \approx 11.4$ μm/s for $\omega/2\pi \approx 200\ s^{-1}$ and $v/\varepsilon \approx 16.5$ μm/s for $\omega/2\pi \approx 550\ s^{-1}$; thickness $d = 50$ μm). For standard parameters of MBBA II we find $v_x^{(0)}/\varepsilon^{1/2} = 16.8$ μm/s, $v_z^{(0)}/\varepsilon^{1/2} = 26.8$ μm/s for $\omega/2\pi \approx 200\ s^{-1}$ (fully rigid boundary conditions). The magnitude of $\sigma_\perp = 7 \times 10^{-8}\ (m\Omega)^{-1}$ was chosen to give a cut-off frequency of about $\omega/2\pi = 700\ s^{-1}$. Obviously the

measured velocity is smaller than what one would expect from our lowest-order theory by a factor between about 6 at $\varepsilon = 0.1$ and 2.8 at $\varepsilon = 0.5$, and the dependence on ε is stronger than predicted. The inclusion of higher-order terms in the ε-expansion probably cannot improve the situation. The reason for this is that, if the terms proportional to ε would become dominant, their contribution would have to exceed that of the $\varepsilon^{1/2}$-terms, which are already too large. The discrepancy is probably not grave, since the experiments are not very accurate, and moreover the particles do not move with maximal velocity along their trajectory. A more significant comparison could presumably be made for the time of revolution.

We point out that in two optical experiments, which should both be sensitive to the amplitude of θ, an $\varepsilon^{1/2}$-behavior was claimed to be found in the range $0.1 \leq \varepsilon \leq 0.5$, and a saturation for larger ε [51, 52]. Whereas Carroll [51] measured in PAA the focal length of the system of rolls, which act as a lattice of cylindrical lenses [44], Kai *et al.* [52] measured in MBBA the intensity of the transmitted polarized monochromatic light. In a very new experiment [53] an $\varepsilon^{1/2}$-behavior of the director orientation was found for $\varepsilon < 0.1$ by measuring the change of the amplitude of the light modulation with ε. We suggest to measure the electric Nusselt number for comparison with our results.

At order ε one obtains contributions to higher spatial harmonics in **u**. Thus the complete expansion of θ, for example, can be written as

$$\theta = \varepsilon^{1/2}[1 + 0(\varepsilon^{1/2})]\, \theta_0(z, t) \cos qx + \\ + \varepsilon\,[1 + 0(\varepsilon^{1/2})]\, \theta_1(z, t) \cos 2\, qx + \ldots \quad (5.10)$$

In our treatment a determination of θ_1, and the corresponding contributions to the other quantities, is included. For fully free boundary conditions and lowest-order time-Fourier expansion one has

$$\theta_0 = \bar{A}_0 \cos z\,, \quad \theta_1 = \bar{A}_1 \sin 2\, z\,. \quad (5.11)$$

For standard parameters of MBBA II we find $\bar{A}_0 = 84.4°$ and $\bar{A}_1 = 16.4°$. The term θ_1 leads to an observable asymmetry in the optical properties sometimes called « squint » [54].

The one-dimensional version of equation (5.4) without Y-derivatives was considered previously for the dc case and fully free boundary conditions [55]. We have only checked the expression for $\xi_\parallel$ and found it to be incorrect.

Of course equation (5.4) can also be applied to the periodic splay-twist instability (then $\xi_\parallel$ and $\xi_\perp$ would be interchanged). We have as yet not determined all parameters for that case.

From the envelope equation (5.4) one can easily show that a two-dimensional wavenumber band of stationary straight-roll solutions exists inside the region $Q^2 + P^2 < 1/3$ (two-dimensional Eckhaus criterion) [8, 9]. This means that, if fluctuations are sufficiently small and effects of boundaries and other disturbances of the ideal system are negligible, all solutions in the stable region should, under appropriate preparation, be experimentally accessible.

Experiments by Lowe and Gollub [56] have essentially verified this for the one-dimensional wavenumber band with $Q^2 < 1/3$ and $P = 0$ (rolls always exactly in the normal direction). Unfortunately fluctuations, which lead to the nucleation of dislocations, appear to be of some importance in the stable region.

It would be very interesting to test also the stability against variations of P, i.e. finite tilt of the rolls with respect to the normal axis. One possible method for such an experiment with appropriate materials would be to prepare tilted rolls by first going to a point in the V-ω-plane where oblique rolls develop spontaneously, and to alter subsequently V and/or ω into the normal-roll regime. One must be aware that lateral boundaries, which are not perpendicular to the roll axis, can lead to additional restrictions as is well-known from quasi-one-dimensional systems [57]. A discussion of boundaries that are perpendicular to the rolls is given in reference [58].

The envelope equation (5.4) can also be used to describe the structure and dynamics of dislocations as well as their nucleation. As pointed out before [9, 59] stationary dislocations exist only at $\mathbf{Q} \equiv (Q, P) = 0$. For $\mathbf{Q} \neq 0$ the direction of motion is perpendicular to **Q** and can therefore take on any direction (« climb » and « glide »). This is different from isotropic systems where glide can occur only in nonpotential situations [60, 61]. There is another essential difference concerning the velocity **V** of a dislocation. Whereas in isotropic systems **V** scales essentially like $Q^{3/2}$ near the band center [60, 61] this nonanalyticity is absent here so that V is essentially proportional to Q. Introducing $X' = X/\xi_\parallel$, $Y' = Y/\xi_\perp$ the results of detailed calculations [59] can be written as $|\mathbf{V}'| = \mu\,|\mathbf{Q}'|$ ($\mathbf{V}' = (V_x/\xi_\parallel, V_y/\xi_\perp)$, $\mathbf{Q}' = (Q\xi_\parallel, P\xi_\perp)$) where for $|\mathbf{V}'| \ll 1$ one has

$$\mu = \begin{cases} 2/\ln\,(R'/1.13) & \text{for } |\mathbf{V}'|\, R' \ll 1 \\ 2/\ln\,(3.29/|\mathbf{V}'|) & \text{for } |\mathbf{V}'|\, R' \gg 1\,. \end{cases} \quad (5.11a)$$

Here R' is the size of the system in the primed units. Equation (5.11a) is valid for $|\mathbf{Q}'| \ll 1$ and $R' \gg 1$.

5.2 OBLIQUE-ROLL REGIME. — For $\omega < \omega_z$ and not too near to the Lifshitz point, where the periodicity at threshold is described by the wavevector $\mathbf{q}_c = (q_c, p_c)$, equation (5.1) has to be generalized to

$$u_i(\mathbf{r}, t) = \varepsilon^{1/2}[U_i\, A(X, Y, T)\, e^{i(q_c x + p_c y)} + \text{cc}] \times \\ \times \tilde{u}_i(z, t) + 0(\varepsilon)\,, \quad (5.12)$$

and the envelope equation reads

$$T_0\,\partial_T A = \\ = [\xi_1^2\,\partial_x^2 + \xi_2^2\,\partial_Y^2 + 2\,\xi_1\,\xi_2\,a\,\partial_X\,\partial_Y + 1 - |A|^2]\,A\,. \quad (5.13)$$

with $|a| < 1$. Similar reasoning as before shows that to lowest nontrivial order the neutral surface is given by

$$\varepsilon = \xi_1^2(q - q_c)^2 + \xi_2^2(p - p_c)^2 + \\ + 2\,\xi_1\,\xi_2\,a(q - q_c)(p - p_c)\,. \quad (5.14)$$

This corresponds to a paraboloid whose principle axes are, in general, not parallel to x and y (and neither in line with the rolls). The quantities T_0, ξ_1, ξ_2 and a can again be determined from the linear analysis.

We have as yet not determined the overall normalization of the $\tilde{u}_i$ in the oblique-roll regime, but work in this direction is in progress. One has here to be aware of a peculiar difficulty that arises when free boundary conditions, that do not provide a surface-torque against twist, are used. Then the preferred axis is defined only by the initial planar alignment. Since oblique rolls actually exert a net torque on the boundaries there is no static solution. The difficulty does not show up in linear order because here the torques balance due to the symmetry $z \to -z$. It would be interesting to perform an experiment with approximately free boundary conditions. Perhaps this can be done by having the nematic material floating on mercury and a free space between the upper surface and the electrode. The resulting rotation can be stopped by applying an axial magnetic field.

The quantities T_0/d^2, ξ_1/d, ξ_2/d and a are plotted in figure 17 for MBBA II (see Appendix D) with modified values of $\varepsilon_a = -0.2$ and $\sigma_\parallel = 2$. For this case ω_z exists. For $\omega > \omega_z$ the corresponding quantities for normal rolls are included. Note that ξ_2 and $\xi_\perp$ vanish at the Lifshitz point and behave as $(\omega_z - \omega)^{1/2}$ in its vicinity. In section 5.3 we derive a connection between a and the derivatives of $\xi_\perp^2$ and ξ_2^2 at $\omega = \omega_z$.

The two-dimensional wavenumber bands for existence and stability now correspond to ellipses centered around (q_c, p_c) and $(q_c, -p_c)$. Since equations (5.4) and (5.13) are mathematically equivalent, all results from the normal-roll case can easily be transferred to the oblique rolls by a rotation of the X, Y-coordinate system. Indications for the two-dimensional stable wavenumber band were obtained by experiments where a given point in the V-ω-plane sufficiently far above threshold and inside the oblique-roll regime was either approached by a sudden jump from the subcritical region ($V < V_c$) or by small voltage steps [6]. In the first case the system

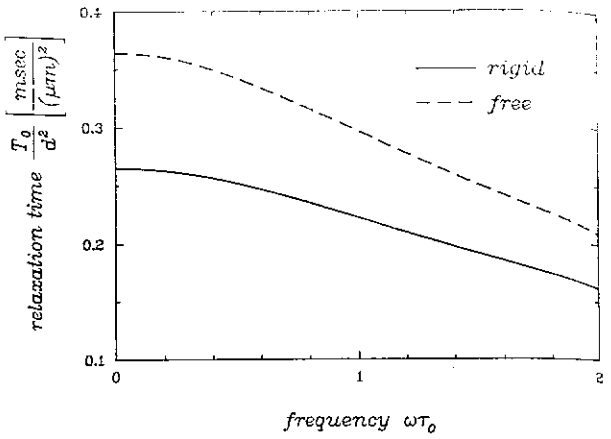

a)

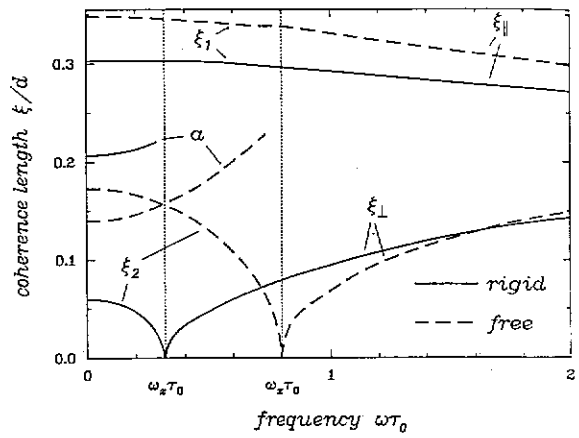

b)

Fig. 17. — The relaxation time T_0 (a) and the coherence lengths $\xi_\parallel$ $\xi_\perp$, ξ_1, ξ_2 and the constant a (b) corresponding to equations (5.4) and (5.13) are plotted as a function of the reduced external frequency $\omega\tau_0$ for free and rigid boundary conditions. Material parameters for MBBA II with modified values of $\varepsilon_a = -0.2$ and $\sigma_\parallel/\sigma_\perp = 2.0$ are used.

settled down at a tilt angle which presumably corresponded more or less to the most-rapidly growing mode, whereas in the second case the system remained locked into the angle corresponding to q_c at threshold. The motion of dislocations is also analogous to the normal-roll case [59].

Domain walls connecting regions with $p \approx p_c$ and $p \approx -p_c$ may be described by two coupled equations of the type (5.13).

We point out that the trajectories of the fluid particles in a roll are closed, even if corrections of order ε are included. This appears to be a result of the symmetry with respect to inversion at the roll axis and is therefore presumably exact for the full nonlinear problem. The flexoelectric terms lead in the case of an applied dc-voltage to helical motion [74].

5.3 VICINITY OF THE LIFSHITZ POINT. — At the Lifshitz point ($\omega = \omega_z$) the prefactors of all Y-derivatives vanish in equations (5.4) and (5.13). Thus for $\omega \approx \omega_z$ a different scaling for Y and a scaled version of $\omega - \omega_z$ may be introduced

$$Y = \varepsilon^{1/4} y\,, \quad \omega - \omega_z = \varepsilon^{1/2}\,\Omega \tag{5.15}$$

(X and T as before). This leads to a different envelope equation

$$T_0\,\partial_T A = [(\xi_1\,\partial_x - i\xi_3^2\,\partial_Y^2)^2 - b\xi_3^4\,\partial_Y^4 + c\Omega\,\xi_3^2\,\partial_Y^2 + 1 - |A|^2]\,A \tag{5.16}$$

with $b > 0$. Here the physical quantities are again given by equation (5.1). T_0 and ξ_1 are the same as before, now taken at $\omega = \omega_z$ (here $\xi_1 = \xi_\parallel$). For q_c in (5.1) one has to take the critical normal-roll wavenumber at the actual ω, or $q_c = q_c(\omega_z) + (\mathrm{d}q_c/\mathrm{d}\omega)(\omega - \omega_z)$. Similarly one must take the normal-roll threshold $V_c(\omega)$ at the actual frequency in the definition (5.2) of ε. The neutral surface described by equation (5.16) is

$$\varepsilon = \xi_1^2(q - q_c)^2 + [2\,\xi_1(q - q_c) + c(\omega - \omega_z)] \times \times\,\xi_3^2 p^2 + (1 + b)\,\xi_3^4 p^4\,. \tag{5.17}$$

For $c(\omega - \omega_z) > 0$ the neutral surface has a minimum at $q = q_c$ and $p = 0$. For very small values of $|q - q_c|$ and $|p|$ one can then approximate (5.17) by

$$\varepsilon = \xi_1^2(q - q_c)^2 + c(\omega - \omega_z)\,\xi_3^2 p^2\,. \tag{5.18}$$

Comparison with equation (5.8) shows that

$$c\xi_3^2 = \partial_\omega \xi_\perp^2\,|_{\omega = \omega_z}\,. \tag{5.19}$$

For $c(\omega - \omega_z) < 0$ the neutral surface has minima at

$$\bar{q}_c = q_c - c(\omega_z - \omega)/2\,b\xi_1\,, \qquad p_c^2 = c(\omega_z - \omega)/2\,b\xi_3^2\,. \tag{5.20}$$

For very small values of $|q - \bar{q}_c|$ and $|p - p_c|$ one can then approximate (5.17) by

$$\varepsilon = -\frac{c^2(\omega_z - \omega)^2}{2\,b} + \xi_1^2(q - \bar{q}_c)^2 + 2\,\frac{1 + b}{b}\,c(\omega_z - \omega)\xi_3^2(p - p_c)^2 + 4\,\sqrt{\frac{c(\omega_z - \omega)}{2\,b}}\,\xi_1\,\xi_3(q - \bar{q}_c)(p - p_c) \tag{5.21}$$

(choose the positive root for $p_c > 0$). Comparing this with equation (5.14) ($\bar{q}_c$ has to be identified with the q_c there) and making use of (5.19) leads to the relations

$$b = 2\,\partial_\omega \xi_\perp^2 / (|\partial_\omega \xi_2^2| - 2\,\partial_\omega \xi_\perp^2)\,, \tag{5.22}$$

$$a^2 = 1 - 2\,\partial_\omega \xi_\perp^2 / |\partial_\omega \xi_2^2|\,, \quad a > 0 \text{ for } p_c > 0\,, \tag{5.23}$$

where a and the quantities on the r.h.s. are to be taken at $\omega = \omega_z$. The quantity ξ_3, which is as yet undetermined, can be obtained from the neutral surface by

$$\xi_3^2 = (4\,\xi_1)^{-1}\,\partial_q\,\partial_p^2(V_0^2/V_c^2)\,. \tag{5.24}$$

From (5.23) one derives the interesting inequality $\partial_\omega \xi_\perp^2 < \frac{1}{2}\,|\partial_\omega \xi_2^2|$ at $\omega = \omega_z$. For standard parameters of MBBA II with $\sigma_\parallel/\sigma_\perp = 2$ and $\varepsilon_a = -0.2$ we find for fully free boundary conditions $\omega_z\,\tau_0 = 0.80$, $\xi_1 = 0.34\,d$, $\xi_3 = 0.16\,d$, $b = 3.23$ and $c = 0.90\,\tau_0$ and for fully rigid boundary conditions $\omega_z\,\tau_0 = 0.32$, $\xi_1 = 0.30\,d$, $\xi_3 = 0.12\,d$, $b = 4.00$ and $c = 0.61\,\tau_0$.

From (5.16) one can deduce interesting stability regions in the q-p-plane for straight-roll solutions, which exhibit the splitting of one stability island on the normal-roll side into two islands on the oblique-roll side [8]. In a small range of Ω there should even exist three separate stability islands. Equation (5.16) also possesses stable undulated (or wavy) normal and slightly oblique roll solutions. They exist in a narrow range inside the oblique-roll regime $c\Omega < 0$ and are in fact less stable than the oblique rolls [8]. The undulated rolls observed experimentally [5, 6] appear to be more stable. Possibly mean-flow effects, which are expected to occur for the undulated rolls, can explain the discrepancy. Work towards inclusion of such effects is in progress.

In the oblique-roll regime equation (5.16) also has domain-wall solutions connecting regions with $p > 0$ and $p < 0$. Their wavevector-selection properties were considered before [9] and are presently under further study. These domain walls may be arranged periodically and then they describe the Zigzag structure observed experimentally [5, 6]. The interaction between well-separated domain walls can be shown to behave in an oscillatory manner, so that many equilibrium positions are possible. This explains the exotic undulated structure observed sometimes [62] and indicates that spatially chaotic states may be expected [63]. Some aspects of the behavior near the normal-oblique transition even far above threshold are captured by a two-dimensional phase-diffusion equation given elsewhere [64].

6. Concluding remarks.

The investigation of the threshold and near-threshold behavior of the electrically (and magnetically) driven pattern-forming instabilities in nematic

liquid crystals presented in this work is a fairly general one. We have mainly used the parameters of MBBA, because this is the only room-temperature nematic exhibiting EHC where most of the parameters are known with some accuracy. However, we have often varied some material parameters to show that various features are independent of the material considered and therefore typical for nematic liquid crystals.

In section 5 the coefficients of the amplitude equations are calculated within the lowest-order time-Fourier approximation. We expect that in situations where the corrections become relevant one would obtain only quantitative changes.

The « full » time-expansion presented in subsection 4.3 was done for rigid boundary conditions only with the trial function approximation for the z-dependence introduced in subsection 3.2 in connection with Appendix A (« approximate rigid boundary conditions »). Meanwhile we were able to test this approximation against an essentially rigorous higher-order Galerkin expansion [76]. We found the corrections to be generally small on the order of a few percent. The most important point in choosing « good » trial functions is apparently to take care of the symmetries, as demonstrated in Appendix A.

The following essential limitations of the presented work remain :

i) We have neglected the flexoelectric effect. For dc voltage it was shown recently that this effect provides an alternative driving force for oblique rolls [73, 74]. This is consistent with the fact that the flexoelectric effect can also lead to a periodic structure that is aligned parallel to the director [75], similar to the periodic splay-twist structure discussed in subsection 4.4. For ac voltages the flexoelectric effect drops out of the lowest-order time-Fourier approximation and therefore its influence is expected to vanish for $d \to \infty$. Preliminary computations with the inclusion of the flexoelectric effect have indeed shown that in the frequency range where the conditions (4.4) and (4.6) hold, the results remain almost unchanged. For smaller thickness the flexoelectric effect becomes more important, but the changes at intermediate frequencies seem to be mainly of quantitative nature. Thus one now has an oblique-roll regime, i.e. $\omega_z > 0$, for standard MBBA [76].

ii) The dielectric regime was not considered explicitly, although the relevant modes are included in our framework. The full threshold behavior including the interaction between the « conduction mode » and the « dielectric mode », which are coupled by the flexoelectric effect, are now under investigation.

We have also looked for Hopf-bifurcations, but never found them to occur as the first (primary) instability. For MBBA-like materials and free or approximate rigid boundary conditions this result can be obtained analytically. With the inclusion of the flexoelectric effect we have as yet found primary Hopf-bifurcations only for very special situations in the frequency range where the conduction mode and the dielectric mode interact strongly [76]. Possibly other generalizations of the basic equations (e.g. charge injection, non-ohmic behavior) have to be invoked in order to describe the observed traveling waves [10].

At this point quantitative discrepancies between our theory and existing experiments should not be taken too seriously. On the one hand the flexoelectric effect does lead to quantitative changes, and on the other hand uncertainties in the experimental arrangements, including uncertainties in the material parameters, are presumably important.

The periodic splay-twist instability was investigated in subsection 4.4 only for a planar configuration without pre-twist in the z-direction. We remark that in a twisted nematic cell one has also a different periodic instability [77] which can compete with the splay-twist instability [16]. We moreover point out that there are quantitative differences between the situations where these static periodic instabilities are driven by a magnetic field or by an electric field [45, 78], which may be important for display design.

From the results of section 5 one can extract the velocity $v = 2\,\xi\,\varepsilon^{1/2}/T_0$ with which a plane wavefront building up the pattern behind it propagates into the unstructured state slightly above threshold [79]. Measurements of this velocity have been performed in the Taylor-Couette [80] and the Rayleigh-Bénard instability [81]. Whereas in the first experiment there is disagreement with theory the latter one shows good agreement. In our case of an anisotropic system the coherence length ξ depends on the direction of propagation.

There is now hope that in the near future a fairly complete and rigorous description of the threshold behavior for EHC and related instabilities is possible. We plan to standardize the relevant computer programs and make them available. This may be important since we have very likely missed interesting scenarios due to the vast size of the parameter space. Moreover we shall persue the investigation of the weakly nonlinear region in order to describe more complicated structures and defects and mean-flow effects [18, 19].

A brief comparison of EHC with thermally driven Rayleigh-Bénard convection in planarly aligned nematics might be in order [82]. Here a convenient second control parameter is a (stabilizing) magnetic field applied parallel to the undistorted director. One may have normal or oblique rolls at zero field (for standard MBBA and boundary conditions that fix the temperature, normal rolls are expected [83, 45]). A weak field first favors normal rolls. At higher

fields (and higher thresholds) a transition to oblique rolls occurs and at very high fields they become « parallel » (wavevector perpendicular to undistorted director). Part of this scenario has been observed [83].

Acknowledgments.

In the course of this work we have benefitted especially from contributions and communications with R. M. Clever, A. Joets, W. Pesch and R. Ribotta. We also wish to thank M. Kaiser, R. B. Meyer, I. Rehberg and W. Thom for useful discussions. This work was supported by the Deutsche Forschungsgemeinschaft (Sonderforschungsbereich 213) and the Emil-Warburg-Stiftung, Bayreuth.

Appendix A.

Trial-function solution for rigid boundary conditions.

We here describe the procedure to determine the constants I_i which have been introduced in equations (3.11-14). For rigid boundary conditions the physical variables can be divided into three classes :

$$\begin{array}{ll} \phi(z),\ \theta(z) : \text{symmetric under } z \to -z\,, & \phi = \theta = 0 \quad \text{at} \quad z = \pm\,\pi/2 \\ v_x(z),\ v_y(z),\ \psi(z) : \text{antisymm. under } z \to -z, & v_x = v_y = \psi = 0 \quad \text{at} \quad z = \pm\,\pi/2 \\ v_z(z) : \text{symmetric under } z \to -z\,, & v_z = \partial_z v_z = 0 \quad \text{at} \quad z = \pm\,\pi/2\,. \end{array} \tag{A.1}$$

Choosing the first (second, third) class proportional to a function $f_1(z)(f_2(z), f_3(z))$ which has the correct symmetry and satisfies the boundary conditions, and projecting (3.2a), (3.2b) onto $f_1(z)$, (3.2c) (3.2d) and (3.2f) onto $f_2(z)$ as well as (3.2e) onto $f_3(z)$ fixes the prefactors and provides the following expressions for the constants I_i :

$$I_1 = -\int_{-\pi/2}^{\pi/2} f_1(z)\,\partial_z^2 f_1(z)\,\mathrm{d}z/J_1\,,$$

$$I_2 = \int_{-\pi/2}^{\pi/2} f_1(z)\,\partial_z f_2(z)\,\mathrm{d}z/J_1\,,$$

$$I_3 = \int_{-\pi/2}^{\pi/2} f_1(z)\,f_3(z)\,\mathrm{d}z/J_1\,,$$

$$I_4 = -\int_{-\pi/2}^{\pi/2} f_2(z)\,\partial_z f_1(z)\,\mathrm{d}z/J_2 = I_2 \cdot J_1/J_2\,,$$

$$I_5 = -\int_{-\pi/2}^{\pi/2} f_2(z)\,\partial_z^2 f_2(z)\,\mathrm{d}z/J_2\,,$$

$$I_6 = -\int_{-\pi/2}^{\pi/2} f_2(z)\,\partial_z f_3(z)\,\mathrm{d}z/J_2\,,$$

$$I_7 = \int_{-\pi/2}^{\pi/2} f_3(z)\,\partial_z f_2(z)\,\mathrm{d}z/J_3 = I_6 J_2/J_3\,,$$

$$I_8 = -\int_{-\pi/2}^{\pi/2} f_3(z)\,\partial_z^2 f_1(z)\,\mathrm{d}z/J_3\,,$$

$$I_9 = I_3 \cdot J_1/J_3\,,$$

$$I_{10} = -\int_{-\pi/2}^{\pi/2} f_3(z)\,\partial_z^3 f_2(z)\,\mathrm{d}z/J_3\,,$$

$$I_{11} = -\int_{-\pi/2}^{\pi/2} f_3(z)\,\partial_z^2 f_3(z)\,\mathrm{d}z/J_3\,, \tag{A.2}$$

with

$$J_i = \int_{-\pi/2}^{\pi/2} f_i^2(z)\,\mathrm{d}z \qquad i = 1, 2, 3\,. \tag{A.3}$$

In particular we have used

$$\begin{aligned} f_1(z) &= \cos z\,, \\ f_2(z) &= \sin 2z\,, \\ f_3(z) &= \frac{\cosh(\lambda_s z)}{\cosh\left(\lambda_s \frac{\pi}{2}\right)} - \frac{\cos(\lambda_s z)}{\cos\left(\lambda_s \frac{\pi}{2}\right)} \end{aligned} \tag{A.4}$$

($\lambda_s = 1.50561873$ (see Ref. [50])). One then obtains $I_1 = 1.0000$, $I_2 = 0.8488$, $I_3 = 1.3948$, $I_4 = 0.8488$, $I_5 = 4.0000$, $I_6 = 1.5724$, $I_7 = 0.7862$, $I_8 = 0.6973$, $I_9 = 0.6973$, $I_{10} = 3.1448$, $I_{11} = 1.2465$.

AppendixB.

The limit $\omega \to 0$.

We here derive the ac threshold in the limit $\omega \to 0$. For simplicity we only consider free boundary conditions and normal rolls ($p = 0$), and the time derivative acting on v_z is neglected, since it is extremely small. For $p = 0$ one only has equations 3.2a, b and d. After replacing ∂_z^2 by -1 and eliminating v_z between 3.2b and d one is left with the following two equations :

$$[-\varepsilon_0(\varepsilon_\parallel q^2 + \varepsilon_\perp)\,\partial_t - (\sigma_\parallel q^2 + \sigma_\perp)]\,\phi + \frac{\sqrt{2}}{\pi}\,\bar{V}\,[\sigma_a + \varepsilon_0\,\varepsilon_a\,\partial_t](q\theta\cos\omega t) = 0\,, \tag{B.1}$$

$$\frac{\sqrt{2}}{\pi}\,\bar{V}\,\varepsilon_0[\varepsilon_a\,\beta_3 + (\varepsilon_\parallel q^2 + \varepsilon_\perp)(\alpha_2 q^2 - \alpha_3)]\,q^2\,\phi\cos\omega t + \\ + \left\{\left[\gamma_1\,\beta_3 - (\alpha_2 q^2 - \alpha_3)^2\,\frac{d^2}{\pi^2}\,\partial_t + \beta_3 K_2 - [\beta_3 + (\alpha_2 q^2 - \alpha_3)\,q^2] * \varepsilon_0\,\varepsilon_a\,2\,\frac{\bar{V}^2}{\pi^2}\cos^2\omega t\right]\right\} q\theta = 0\,. \tag{B.2}$$

These two coupled first-order differential equations can be transformed into one second-order equation of the form

$$[\partial_t^2 + g_1(t)\,\partial_t + g_0(t)]\,\theta = 0\,. \qquad \text{(B.3)}$$

We need the quantities g_0 and g_1 only for $\omega \to 0$. Then one finds

$$g_1 = \left[1 + \frac{\tau}{\tau_d}\,(1 + 2(\bar{V}^2/B)\cos^2\omega t)\right]/\tau\,,$$
$$g_0 = [1 - 2(\bar{V}^2/V_{dc}^2)\cos^2\omega t]/\tau_d\,\tau\,, \qquad \text{(B.4)}$$

where the charge relaxation time τ and the director relaxation time τ_d are given in (3.13) and (4.4), and the dc threshold V_{dc} is obtained by (3.11) with $\omega = 0$. B is given by

$$B = -\frac{\pi^2 K_2}{\varepsilon_0\,\varepsilon_a}\,\frac{\varepsilon_\parallel\,q^2 + \varepsilon_\perp}{\varepsilon_\perp\,(1+q^2)}\,. \qquad \text{(B.5)}$$

In the limit $\omega \to 0$ we solve (B.3) by a WKB-Ansatz $\theta = \exp(S(\omega\,.\,t)/\omega)$ with $S = S_0 + \omega S_1 + \ldots$ To order ω^0 one immediately obtains

$$\dot{S}_0^2 + g_1\,\dot{S}_0 + g_0 = 0 \qquad \text{(B.6)}$$

which yields

$$2\,\dot{S}_0 = -\,g_1 + \sqrt{g_1^2 - 4\,g_0}\,. \qquad \text{(B.7)}$$

Clearly the growth rate (Floquet coefficient in equation (3.7)) is given by the average of $\dot{S}_0$ over one period : $\sigma = \langle \dot{S}_0 \rangle$. Inserting (B.4) into (B.7) and requiring $\langle \dot{S}_0 \rangle = 0$ determines the threshold $\bar{V}_0^2$ at $\omega = 0$. For $\tau/\tau_d \ll 1$ one finds

$$\bar{V}^2 = V_{dc}^2\left[1 + \frac{\tau}{\tau_d}\,(V_{dc}^2/2\,B + 4) + 0\left(\left(\frac{\tau}{\tau_d}\right)^2\right)\right]. \qquad \text{(B.8)}$$

Appendix C.

Rigorous treatment of time dependence.

Here we include higher-order time-Fourier terms but keep the treatment of the z-dependence as in section 3.2 in connection with Appendix A. A recursion relation for the determination of the threshold is derived and transformed into a continued fraction.

Eliminating from the six coupled equations (3.2) for the n-th Fourier mode (see Eqs. (3.8)) the quantities ϕ_n, ψ_n, v_{xn}, v_{yn} and v_{zn}, the following recursion relation for θ can be obtained

$$F_n\,\theta_n + G_n\,\theta_{n+1} + H_n\,\theta_{n-1} = 0 \qquad \text{(C.1)}$$

with

$$F_n = [Z_1^n\,Y_3^n + (Z_6^n + Z_6^{n-1} - Z_8^n)\,Y_1^n]\,Z_5^n + \\ + p^2[Z_1^n\,Z_7^n\,Y_2^n + Z_3^n\,Z_4^n\,Y_3^n - Z_4^n\,Z_7^n\,Y_1^n \\ + Z_3^n(Z_6^n + Z_6^{n-1} - Z_8^n)\,Y_2^n]$$
$$G_n = [Z_2^n\,Y_3^n + Z_6^n\,Y_1^n]\,Z_5^n + p^2[Z_2^n\,Z_7^n + Z_3^n\,Z_6^n]\,Y_2^n$$
$$H_n = [Z_2^{n-1}\,Y_3^n + Z_6^{n-1}\,Y_1^n]\,Z_5^n + \\ + p^2[Z_2^{n-1}\,Z_7^n + Z_3^n\,Z_6^{n-1}]\,Y_2^n \qquad \text{(C.2)}$$

and

$$Y_1^n = \alpha_2\,I_3\,q^2 - \alpha_3\,I_2\,I_6 - \alpha_3\,p^2\,I_3\,\mu_1^n/\mu_2^n$$
$$Y_2^n = \alpha_3\,I_6 + (\alpha_3\,p^2 - \alpha_2\,q^2)\,\mu_1^n/\mu_2^n$$
$$Y_3^n = \mu_3^n + p^2\,\mu_1^n\,\mu_4^n/\mu_2^n \qquad \text{(C.3)}$$

$$Z_1^n = \lambda_{2n}\frac{d^2}{\pi^2}\left(\gamma_1 + \alpha_3^2 p^2 \frac{I_2\,I_4}{\mu_2^n}\right) + \\ + K_2 - \varepsilon_0\,\varepsilon_a\frac{\bar{V}^2}{2\,\pi^2}\,[2 - q^2(U_n + U_{n-1})]$$
$$Z_2^n = -\,\frac{1}{2}\,\varepsilon_0\,\varepsilon_a\frac{\bar{V}^2}{\pi^2}\,(1 - q^2\,U_n)$$
$$Z_3^n = \left[\lambda_{2n}\frac{d^2}{\pi^2}\,(\alpha_2\,q^2 - \alpha_3\,p^2)\,\alpha_3/\mu_2^n + k_{11} - k_{22}\right] I_2$$
$$Z_4^n = Z_3\,I_4/I_2$$
$$Z_5^n = \lambda_{2n}\frac{d^2}{\pi^2}\,[\gamma_1 - (\alpha_3\,p^2 - \alpha_2\,q^2)^2/\mu_2^n] + K_1$$
$$Z_6^n = \varepsilon_0\frac{\bar{V}^2}{2\,\pi^2}\,[(\varepsilon_\parallel\,q^2 + \varepsilon_\perp\,p^2 + \varepsilon_\perp\,I_1)\,U_n - \varepsilon_a]\,q^2$$
$$Z_7^n = -\,\lambda_{2n}\frac{d^2}{\pi^2}\,[-\,\alpha_3\,I_4 + (\alpha_2\,q^2 - \alpha_3\,p^2)\,\mu_4^n/\mu_2^n]$$
$$Z_8^n = \lambda_{2n}\frac{d^2}{\pi^2}\,[\alpha_2\,I_8\,q^2 - \alpha_3\,I_2\,I_6 + \alpha_3\,p^2\,I_4\,\mu_4^n/\mu_2^n]\,, \qquad \text{(C.4)}$$

$$\mu_1^n = -\,\lambda_{2n}\frac{d^2}{\pi^2}\rho_m\,I_6 - \beta_1\,,$$
$$\mu_2^n = \lambda_{2n}\frac{d^2}{\pi^2}\rho_m(q^2 + p^2) + \beta_2\,,$$
$$\mu_3^n = \lambda_{2n}\frac{d^2}{\pi^2}\rho_m(q^2 - I_6\,I_7) + \beta_3\,,$$
$$\mu_4^n = \lambda_{2n}\frac{d^2}{\pi^2}\rho_m\,I_7 + \beta_1' \qquad \text{(C.5)}$$

$$U_n = (\sigma_a\,\sigma_\perp^{-1}S^{-1} + \varepsilon_a\,\varepsilon_\perp^{-1}D_1^{-1}\lambda_{2n+1}\,\tau)/ \\ (1 + \lambda_{2n+1}\,\tau)\,, \qquad \text{(C.6)}$$

$$\lambda_m = \lambda + \mathrm{i}n\,\omega\,. \qquad \text{(C.7)}$$

The recursion relation (C.1) can be transformed into

$$F_0 - 2\,\mathrm{Re}\,[G_0 H_1/K_e] = 0\,, \qquad \text{(C.8)}$$

$$K_e = F_1 - \cfrac{G_1 H_2}{F_2 - \cfrac{G_2 H_3}{F_3 - \dots}}\,. \qquad \text{(C.9)}$$

The integral $I_1 \dots I_{11}$ are defined in Appendix A and are for fully free boundary conditions all equal to 1. For given material parameters and wavenumbers q and p, equation (C.8) is an implicit condition for the growth rate $\sigma(q, p\,;\bar{V}, \omega)$, and from $\sigma = 0$ the neutral surface $V_0(q, p\,;\omega)$ is obtained. the continued fraction K_e can be calculated by standard methods [65].

The recursion scheme presented above is easily programmable on a (small) computer and reduces the computation time compared to that needed for naive solution of the problem considerably. One would then deal with $10\,n + 6$ coupled real algebraic equations where n is the order of the Fourier expansion. Equation (C.1) is equivalent to a homogeneous system of algebraic equations with a tridiagonal matrix. There exist efficient algorithms [66] to solve such tridiagonal systems which take nearly twice the computation-time as the method with continued fractions, but have the advantage that the symmetry in equation (3.8) is not needed and therefore is also appropriate for the calculation of the Hopf-bifurcation.

For a harmonic driving field higher-order Fourier components were considered previously within the one-dimensional model by Sengupta and Saupe [34]. For a square-wave driving field rigorous treatment of the time-dependence was introduced within the one-dimensional model by Dubois-Violette [67, 68]. Generalization to two dimensions for free boundary conditions has been also done [69, 70].

Appendix D.

Material parameter.

The following two sets of the material parameters for the nematic liquid-crystal material MBBA (*N*-(*p*-methoxybenzylidene)-*p*-butylamiline) are used :

Material parameter	MBBA I	MBBA II
k_{11}	6.66	6.1
k_{22}	4.2	4
k_{33}	8.61	7.25
α_1	− 18.1	6.5
α_2	− 110.4	− 77.5
α_3	− 1.1	− 1.2
α_4	82.6	83
α_5	77.9	46
α_6	− 33.6	− 35
$\varepsilon_\parallel$	4.72	4.72
$\varepsilon_\perp$	5.25	5.25
$\sigma_\parallel/\sigma_\perp$	1.5	1.5

The rotational viscosities γ_1 and γ_2 are defined in equation (2.13). The often used shear viscosities η_1 $(= \eta_c)$ and η_2 $(= \eta_b)$ are given in equation (3.4), and $\eta_a = \alpha_4/2$ [2, 26]. The elasticities k_{ii} are given in units of 10^{-12} N and the viscosities in units of 10^{-3} kg m^{-1} s^{-1}. For MBBA I the values for the elastic constants are taken from reference [71] and the values for the viscosities from reference [72] at 25 °C. The parameters for MBBA II are taken from the reference [41]. If not stated otherwise we have used for the conductivity $\sigma_\perp = 10^{-8}\,\Omega^{-1}\,\mathrm{m}^{-1}$. In cases where the dielectric tensor was varied, its trace was kept constant at $\bar{\varepsilon} = (2\,\varepsilon_\perp + \varepsilon_\parallel) = 15.22$.

References

[1] Goossens, W. J. A., *Advances Liquid Cryst.*, G. H. Brown, Ed. (Academic Press) **3** (1978) 1.

[2] Blinov, L. M., Electro-Optical and Magneto-Optical Properties of Liquid Crystals (Wiley, New York) 1983.

[3] Joets, A., Yang, X. D. and Ribotta, R., *Physica* **23D** (1986) 235.

[4] Yamazaki, H., Kai, S. and Hirakawa, K., *J. Phys. Soc. Jpn* **56** (1987) 1.

[5] Joets, A. and Ribotta, R., Cellular Structures in Instabilities, J. E. Wesfreid and S. Zaleski, Eds. (Springer, Berlin) 1984, p. 294 ;
Ribotta, R., Joets, A. and Lin Lei, *Phys. Rev. Lett.* **56** (1986) 1595.

[6] Joets, A. and Ribotta, R., *J. Phys. France* **47** (1986) 595.

[7] See e.g. Busse, F. H., Hydrodynamic Instabilities and the Transition to Turbulence, H. L. Swinney and J. P. Gollub, Eds., 2nd Ed. (Springer, Berlin) 1986 ;
Normand, C., Pomeau, Y. and Velarde, M. G., *Rev. Mod. Phys.* **49** (1977) 581.

[8] Pesch, W. and Kramer, L., *Z. Phys.* **B 63** (1986) 121.

[9] Kramer, L., Bodenschatz, E., Pesch, W. and Zimmermann, W., The Physics of Structure Formation, W. Güttinger and G. Dangelmayr, Eds. (Springer, Berlin) 1987.

[10] Joets, A. and Ribotta, R., Propagation in nonequilibrium systems, J. E. Wesfreid, Ed. (Springer) 1988 ;
Rehberg, I., Rasenat, S. and Steinberg, V., preprint, 1988.

[11] See e.g. Newell, A. C., Propagation in nonequilibrium systems, J. E. Wesfreid, Ed. (Springer) 1988 and references cited therein.

[12] See e.g. HOHENBERG, P. C. and CROSS, M. C., Fluctuations and Stochastic Phenomena in Condensed Matter, L. Garrido Ed., *Lect. Notes Phys.* 268 (Springer, Berlin) 1987 and references cited therein.

[12a] MEYER, R. B., *Phys. Rev. Lett.* **22** (1969) 918 ; PROST, J. and MARCEROU, J. P., *J. Phys. France* **38** (1977) 315.

[13] ZIMMERMANN, W. and KRAMER, L., *Phys. Rev. Lett.* **55** (1985) 402.

[14] LONBERG, F. and MEYER, R. B., *Phys. Rev. Lett.* **55** (1985) 718.

[15] OLDANO, C., *Phys. Rev. Lett.* **56** (1986) 1098. MIRALDI, E., OLDANO, C. and STRIGAZZI, A., *Phys. Rev.* **A 34** (1986) 4348.

[16] KINI, U. D., *J. Phys. France* **47** (1986) 693 ; **47** (1986) 1829 ; **48** (1987) 1187 ; **49** (1988) 527.

[17] ZIMMERMANN, W. and KRAMER, L., *Phys. Rev. Lett.* **56** (1986) 2655.

[18] DAVEY, A., HOCKING, L. M. and STEWARTSON, K., *J. Fluid Mech.* **63** (1974) 529.

[19] ZIPPELIUS, A. and SIGGIA, E. D., *Phys. Rev.* **A 26** (1982) 1788 ; *Phys. Fluids* **26** (1983) 2905 ; CROSS, M. C., *Phys. Rev.* **A 27** (1983) 490 ; BUSSE, F. H. and BOLTON, E. W., *J. Fluid Mech.* **146** (1984) 115 ; BERNOFF, A. J. (preprint 1986).

[20] OSEEN, C. W., *Ark. Mat. Astron. Fys.* **A 19** (1925) 1 ; *Fortschr. Chem. Phys. Phys. Chem.* **20** (1929 1 ; *Trans. Faraday Soc.* **29** (1933) 883.

[21] ZOCHER, H., *Trans. Faraday Soc.* **29** (1933) 945.

[22] FRANK, F. C., *Discuss. Faraday Soc.* **25** (1958) 19.

[23] CHANDRASEKHAR, S., Liquid Crystals (Cambridge University Press, London) 1977.

[24] ERIKSON, J. L., *Arch. Ration. Mech. Analysis* **23** (1966) 266.

[25] LESLIE, F. M., *Quart. J. Mech. Appl. Math.* **19** (1966) 357.

[26] DE GENNES, P. G., The physics of Liquid Crystals (Clarendon, Oxford, England) 1974.

[27] DUBOIS-VIOLETTE, E., DURAND, G., GUYON, E., MANNEVILLE, P. and PIERANSKI, P., *Solid State Phys.*, L. Liebert Ed. (Academic Press) 1978 Suppl. 14.

[28] PARODI, O., *J. Phys. France* **31** (1970) 581.

[29] MARTIN, P. C., PARODI, O. and PERSHAN, P. J., *Phys. Rev.* **A 6** (1971) 1016.

[30] CESARI, L., Asymptotic behavior and stability problems in ordinary differential equations (Springer, Berlin) 1971.

[31] Orsay Liquid Crystals Group, *Phys. Rev. Lett.* **26** (1970) 1642.

[32] DUBOIS-VIOLETTE, E., DE GENNES, P. G. and PARODI, O., *J. Phys. France* **32** (1971) 305.

[33] PIKIN, S. A., *Zh. Eksp. Teor. Fiz.* **60** (1971) 1185 [*Sov. Phys.-JETP* **33** (1971) 641] ; *Zh. Eksp. Teor. Fiz.* **61** (1971) 2133 [*Sov. Phys. JEPT* **34** (1972) 1137].

[34] SENGUPTA, P. and SAUPE, A., *Phys. Rev.* **A 9** (1974) 2698.

[35] PENZ, P. A. and FORD, G. W., *Phys. Rev.* **A 6** (1972) 414.

[36] HELFRICH, W., *J. Chem. Phys.* **51** (1969) 4092.

[37] MEYERHOFER, D., Introduction to Liquid Crystals. E. B. Priestly, P. J. Wojtowitz and Ping Sheng Eds. (Plenum Press, New York) 1975.

[38] KRAMER, L., SCHOBER, H. and ZIMMERMANN, W., *Physica D* **31** (1988) 212.

[39] See e.g. GUCKENHEIMER, J. and HOLMES, P., Nonlinear Oscillations, Dynamical Systems and Bifurcations of Vector Fields (Springer, Berlin) 1983, Chap. 7.

[40] MANNEVILLE, P. and DUBOIS-VIOLETTE, E., *J. Phys. France* **37** (1976) 285.

[41] STEPHEN, M. J. and STRALEY, J. P., *Rev. Mod. Phys.* **46** (1974) 617.

[42] TEANEY, D. T. and MIGLIORI, M., *J. Appl. Phys.* 41 (1970) 998.

[43] WILLIAMS, R., *J. Chem. Phys.* **39** (1963) 384.

[44] PENZ, A., *Phys. Rev. Lett.* **24** (1970) 1405.

[45] ZIMMERMANN, W., Ph. D. Thesis, Universität Bayreuth (1987).

[46] HURD, A. J., FRADEN, S., LONBERG, F. and MEYER, R. B., *J. Phys. France* **46** (1985) 905.

[47] HILSUM, C. and SAUNDERS, F. C., *Mol. Cryst. Liq. Cryst.* **64** (1980) 25.

[47a] KAI, S., Noise in nonlinear dynamical systems, P. V. E. McClintock and F. Moss Eds. (Cambridge Univ. Press, Cambridge) 1987.

[47b] JOETS, A., thèse de 3e cycle, Université Paris-7 (1984).

[48] DE JEU, H. W. and VAN DER VEEN, J., *Phys. Lett.* **A 44** (1973) 277.

[49] SEGEL, L. A., *J. Fluid Mech.* **38** (1969) 203 ; NEWELL, A. C. and WHITEHEAD, J. A., *J. Fluid Mech.* **38** (1969) 279.

[49a] BODENSCHATZ, E., Diploma-thesis, Universität Bayreuth (1985).

[50] CHANDRASEKHAR, S., Hydrodynamic and Hydromagnetic Stability (Clarendon Press, Oxford) 1961.

[51] CARROLL, T. O., *J. Appl. Phys.* **43** (1972) 1342.

[52] KAI, S., ARAOKA, M., YAMAZAKI, H. and HIRAKAWA, K., *J. Phys. Soc. Jpn* **46** (1979) 383.

[53] RASENAT, S., HARTUNG, G., WINKLER, B. L. and REHBERG, I., Exp. in Fluids, in press.

[54] BEN-ABRAHAM, S. I., *J. Phys. Colloq. France* **40** (1979) C 3-259.

[55] HIJIKURO, N., *Prog. Theor. Phys.* **54** (1975) 592.

[56] LOWE, M. and GOLLUB, J. P., *Phys. Rev. Lett.* **55** (1985) 2575.

[57] CROSS, M. C., DANIELS, P. G., HOHENBERG, P. C. and SIGGIA, E. D., *Phys. Rev. Lett.* **45** (1980) 898 ; *J. Fluid Mech.* **127** (1983) 155 ; KRAMER, L. and HOHENBERG, P. C., *Physica* **13D** (1984) 357 ; HOHENBERG, P. C., KRAMER, L. and RIECKE, H., *Physica* **15D** (1983) 402.

[58] BODENSCHATZ, E. and KRAMER, L., *Physica* **27D** (1987) 249.

[59] BODENSCHATZ, E., PESCH, W. and KRAMER, L., *Physica D*, in press.

[60] SIGGIA, E. D. and ZIPPELIUS, A., *Phys. Rev.* **A 24** (1981) 1036 ; POMEAU, Y., ZALESKI, S. and MANNEVILLE, P., *Phys. Rev.* **A 27** (1983) 2710.

[61] TESAURO, G. and CROSS, M. C., *Phys. Rev.* **A 34** (1986) 1363.
[62] RIBOTTA, R., private communication.
[63] COULLET, P., ELPHIK, C. and REPAUX, D., *Phys. Rev. Lett.* **58** (1987) 431.
[64] KRAMER, L., ZIMMERMANN, W., BODENSCHATZ, E. and PESCH, W., Propagation in nonequilibrium systems, J. E. Wesfreid Ed. (Springer) 1988.
[65] ABRAMOWITZ, M. and STEGUN, I. A., Handbook of Mathematical Functions (Dover, New York) 1964 Chap. 3.
[66] SMITH, G. D., Numerical Solution of Partial Differential Equations : Finite Difference Methods (Clarendon, Oxford) 1985.
[67] DUBOIS-VIOLETTE, E., *J. Phys. France* **33** (1972) 95.
[68] SMITH, I. W., GALERNE, Y., LAGERWALL, S. T., DUBOIS-VIOLETTE, E. and DURAND, G., *J. Phys. Colloq. France* **36** (1975) C 1-237.
[69] CHIGRINOV, V. G. and PIKIN, S. A., *Kristallografiya* **23** (1978) 333 ; [*Sov. Phys. Crystallogr.* **23** (1978) 184].
[70] RIGOPOULOS, R. A. and ZENGINOGLOU, H. M., *Mol. Cryst. Liq. Cryst.* **35** (1976) 307 ;
ZENGINOGLOU, H. M., RIGOPOULOS, R. A. and KOSMOPOULOS, I. A., *Mol. Cryst. Liq. Cryst.* **39** (1977) 27 ;
ZENGINOGLOU, H. M. and KOSMOPOULOS, I. A., *Mol. Cryst. Liq. Cryst.* **43** (1977) 265.
[71] DE JEU, H. W., CLAASSEN, W. A. P. and SPRUYIT, A. M. J., *Mol. Cryst. Liq. Cryst.* **37** (1976) 269.
[72] KNEPPE, H., SCHNEIDER, F. and SHARMA, N. K., *J. Chem. Phys.* **77** (1982) 3203.
[73] MADHUSUDANA, N. V., RAGHUNATHAN, V. A. and SUMATHY, K. R., *Pramana J. Phys.* **28** (1987) L 311. There are some misprints in Eqs. (5) and (7).
[74] THOM, W., ZIMMERMANN, W. and KRAMER, L. (preprint 1988).
[75] BOBYLEV, Yu. P. and PIKIN, S. A., *Zh. Eksp. Teor. Fiz.* **72** (1977) 369 [*Sov. Phys. JETP* **45** (1977) 195] ;
BARNIK, M. I., BLINOV, L. M., TRUFANOV, A. N. and UMANSKII, B. A., *Zh. Eksp. Teor. Fiz.* **73**, 1936 (1977) [*Sov. Phys. JETP* **46** (1977) 1016].
[76] ZIMMERMANN, W. and THOM, W., to be published.
[77] CHIGRINOV, V. V., BELYAEV, V. V., BELYAEV, S. V. and GREBENKIN, M. F., *Zh. Eksp. Teor. Fiz.* **77** (1977) 2081 [*Sov. Phys. JETP* **50** (1979) 994] ;
UMANSKII, B. A., CHIGRINOV, V. G., BLINOV, L. M. and POD'YACHEV, Yu. B., *Zh. Eksp. Fiz.* **81** (1981) 1307 [*Sov. Phys. JETP* **54** (1981) 694].
[78] ZIMMERMANN, W. and BAUR, G., to be published.
[79] BEN-JACOB, E., BRAND, H., DEE, G., KRAMER, L. and LANGER, J. S., *Physica* **14D** (1985) 348.
[80] AHLERS, G. and CANNELL, D., *Phys. Rev. Lett.* **50** (1983) 1583.
[81] FINEBERG, J. and STEINBERG, V., *Phys. Rev. Lett.* **58** (1987) 1332.
[82] DUBOIS-VIOLETTE, E., GUYON, E. and PIERANSKI, P., *Mol. Cryst. Liq. Cryst.* **26** (1973) 193.
[83] JOETS, A., KRAMER, L., RIBOTTA, R., SALAN, J. and ZIMMERMANN, W., to be published.